SUB 750-WATT ELECTRIC PROPULSION DYNAMOMETER

A Thesis by

Yrithu Thulaseedharan Pillay

Bachelor of Aerospace Engineering and Mechanics, University of Minnesota, 2016

Submitted to the Department of Aerospace Engineering
and the faculty of the Graduate School of
Wichita State University
in partial fulfillment of
the requirements for the degree of
Master of Science

December 2018

© Copyright 2018 by Yrithu Thulaseedharan Pillay

All Rights Reserved

SUB 750-WATT ELECTRIC PROPULSION DYNAMOMETER

The following faculty members have examined the final copy of this thesis for form and content, and recommend that it be accepted in partial fulfillment of the requirement for the degree of Master of Science, with a major in Aerospace Engineering.

_____

L. Scott Miller, Committee Chair

_____

James E. Steck, Committee Member

_____

Ward T. Jewell, Committee Member

DEDICATION

To my parents, and my brother.

Necessity is the mother of invention.

ACKNOWLEDGEMENTS

I would first like to thank my advisor Dr. L. Scott Miller for his guidance and support. Dr. Miller allowed me to develop and build the design on my own and helped me when I ran into trouble. I also would like to thank my committee members Dr. Ward T. Jewell and Dr. James E. Steck for their tremendous input and feedback.

Secondly, I would like to thank my parents and my brother without whom this thesis would not have been possible. They taught me to never give up and helped me stay focused even when I was ready to give up.

Thanks are also due for Kevin Hagen and Vijay Matheswaran for their tremendous help with manufacturing components, helping me bounce ideas, discussing concepts, and sharing your knowledge about sensor design and data acquisition. Finally, I would like to thank Matthew Decker for his help calibrating sensors.

ABSTRACT

The recent surge in popularity of small electric UAVs under 2kg (4 lbs.) has exposed a need for reliable electric motor performance data. With these UAVs using propulsion systems below 750 W, the systems designed to test bigger motors cannot be used. Moreover, there exists no standard form in which this data can be used for aerospace design.

Existing data for the propulsion system components were studied and the parameters necessary to characterize the motor have been identified. A test system has been designed and built to obtain these parameters. The system is capable of testing a motor under 27,000 RPM running at up to 18.5 V and 45 A at a maximum of 750 W. The system's capability to produce repeatable, and reliable data has been proven. A method to use the obtained data in conjunction with other propulsion system data to characterize the full system and to identify an optimal propulsion system for a UAV design has also been devised. Moreover, the limitations and necessary conditions for the tests have been laid out.

TABLE OF CONTENTS

Chapter Page

1. INTRODUCTION 1

1.1. Background 1
1.2. Importance of propulsion system performance data 1
1.3. Existing techniques and problems 2
1.4. Goals 4

2. THEORY 5

2.1. Conceptual design routine 5
2.2. The battery 5
2.3. The propeller 7
2.4. The motor 9
2.4.1. Types of electric motors 9
2.4.2. Motor model 11
2.5. The electronic speed controller 13
2.6. The system 14

3. TEST APPARATUS 15

3.1. Apparatus concept 15
3.2. Apparatus overview 16
3.3. Power supply and electronic load 17
3.4. Sensors 18
3.4.1. Voltage sensor 18
3.4.2. Current sensor 19
3.4.3. Torque sensor 19
3.4.4. RPM sensor 22
3.4.5. Temperature sensors 24
3.5. Data acquisition 24
3.6. Calibration 25
3.6.1. Voltage sensor 25
3.6.2. Current sensor 26
3.6.3. Torque sensor 27
3.6.4. RPM sensor 29
3.6.5. Temperature sensors 29
3.7. Uncertainties and sensitivity analysis 29
3.8. Limitations 34

TABLE OF CONTENTS (continued)

Chapter Page

4. PROCEDURE 36

4.1. Pre-test requirements 36
4.2. Test procedure 36
4.3. Test outputs 37

5. RESULTS AND DISCUSSION 38

5.1. Repeatability 39
5.2. Further tests 44
5.2.1. Varying ESC 44
5.2.2. Varying $\boldsymbol{Vmec}$ 47
5.2.3. Lower power motor 48
5.2.4. Higher power motor 50
5.2.5. Varying throttle setting 51
5.3. Quick comparison of motor-ESC combos 53
5.4. Other observations 55
5.4.1. Cold test case 55
5.4.2. Temperature effects 56
5.4.3. Testing high power motors 56
5.4.4. Running a motor beyond its ratings 57

6. CONCLUSIONS 58

7. RECOMMENDATIONS 59

7.1. Torque sensor data rate 59
7.2. In-house current sensor 59
7.3. Simplified torque sensor design 60

REFERENCES 62

APPENDICES 64

A. WSU MOTOR TESTING SYSTEM USER MANUAL 65

B. COLD TEST DATA 74

LIST OF TABLES

Table Page

1. The Maximum Expected Sensor Uncertainties 30

2. The Limitations of The Motor Test Stand Components 34

LIST OF FIGURES

Figure Page

1. An illustrative efficiency curve for an electric motor overlaid with two illustrative propeller efficiency curves... 3

2. Battery testing apparatus used at Wichita State University. 6

3. Performance history of *Great Planes Electrifly 3S 850 mAh* LiPo battery 6

4. Performance data for an EAPC 12x12 propeller. 8

5. Dimensionalized performance data for the EAPC 12x12 propeller at $\rho = 1.225\ kg.m^{-3}$ and $U = 15\ m.s^{-1}$ 9

6. Various types of DC electric motors 9

7. Brushless ESCs of varying current ratings 13

8. Overview of the motor test apparatus. 16

9. The test section and its various components 16

10. The power supply and the electronic load 17

11. Schematic of the voltage divider circuit designed to measure V_{mec} 19

12. The system used to measure Q_m 20

13. The bearing used in the torque sensor 20

14. Some designs that were attempted to measure Q_m 21

15. The RPM sensor setup along with the load motor 23

16. The signal from the RPM sensor, along with the pseudo-digital signal 24

17. The calibration curve obtained for the voltage sensor. 25

18. The calibration curve obtained for the current sensor 26

LIST OF FIGURES (continued)

Figure Page

19. Torque calibration technique 27

20. The calibration curve obtained for the torque sensor 28

21. Percentage full scale error observed in the torque measurements 31

22. Percentage error observed in the voltage measurements 32

23. Percentage error observed in the current measurements 33

24. The test stand that incorporates all the required equipment 38

25. Performance data for the *Rimfire 400* with the *Talon 25A*, tested at $11.0\ V$ 40

26. The sensed V_{mec} for the *Rimfire 400* with the *Talon 25A*, tested at $11.0\ V$ 41

27. Performance data for the *Scorpion SII-2212-1400KV* with the *Electrifly 45A*, tested at $11.1\ V$ 42

28. The sensed V_{mec} for the *Scorpion SII-2212-1400KV* with the *Electrifly 45A*, tested at $11.1\ V$ 43

29. Performance data for the *Rimfire 400* with the *Electrifly 25A*, tested at $11.0\ V$ 45

30. Performance data for the *Scorpion SII-2212-1400KV* with the *Phoenix 75A*, tested at $11.1\ V$ 46

31. Performance data for the *Rimfire 400* with the *Electrifly 25A*, tested at $7.4\ V$. 48

32. Performance data for the *Rimfire 370* with the *Talon 25A*, tested at $11.1\ V$ 49

33. Performance data for the *Rimfire .10* with the *Electrifly 45A*, tested at $11.1\ V$ 51

LIST OF FIGURES (continued)

Figure Page

34. Performance data for the *Rimfire 370* with the *Talon 25A*, tested at $11.1\ V$ for varying throttle settings. 53

35. Comparison of performance data for all the tested motors 54

36. Schematic of a possible in-house current sensor 59

37. Schematic of a possible simplified torque sensor 61

38. Performance data for the *Rimfire 400* with the *Electrifly 25A*, tested at $11.0\ V$ along with the cold test data. 74

39. Performance data for the *Scorpion SII-2212-1400KV* with the *Electrifly 45A*, tested at $11.1\ V$ along with the cold test data. 75

LIST OF ABBREVIATIONS

ADC	Analog to Digital Converter
DC	Direct Current
EMF	Electromagnetic Field
ESC	Electronic Speed Controller
LiPo	Lithium Polymer
MOSFET	Metal-Oxide-Semiconductor Field-Effect Transistor
PWM	Pulse Width Modulated (Modulation)
S	Cells in Series
UAV	Unmanned Aerial Vehicle

LIST OF SYMBOLS

A	Ampere
$A.h$	Ampere hour
C_{P_p}	Propeller shaft power coefficient
C_{Q_p}	Propeller torque coefficient
C_{T_p}	Propeller thrust coefficient
η_m	Motor efficiency
η_{mec}	Motor-ESC combo efficiency
η_p	Propeller Efficiency
η_{sys}	System efficiency
F_{LC}	Force at the load cell
Hz	Hertz
I_0	Current at zero load
I_{batt}	Current drwan from battery
I_{in_m}	Motor input current
I_{max}	Maximum current for the motor-ESC combo
I_{mec}	Motor-ESC combo current input
I_{shunt}	Current through shunt resistor
J	Advance Ratio
K_t	Motor torque constant
K_v	Motor speed constant

LIST OF SYMBOLS (continued)

$mA.h$	milli Ampere hour
mec	Motor-ESC combo
n	Revolutions per second
Ω_m	Motor angular velocity
Ω_p	Propeller angular velocity
P_{in}	Motor electric input power
P_{max}	Maximum power for the mc
P_{out_m}	Motor mechanical output power
P_p	Propeller shaft power
P_{shunt}	Power in shunt resistor
Q_m	Motor torque
$Q_{m_{ideal}}$	Motor torque under ideal conditions
Q_p	Propeller torque
R	Calcualted quantity
R_m	Motor resistance
R_{shunt}	Resistance of the shunt resistor
ρ	Air density
RPM	Revolutions Per Minute
$RPM_{m_{ideal}}$	Motor RPM under ideal conditions
RPM_p	Propeller RPM

LIST OF SYMBOLS (continued)

s	seconds
T_m	Test motor temperature
T_p	Propeller Thrust
T_r	Room temperature
U	Free Stream Velocity
V	Volts
V_{batt}	Battery voltage
V_{in_m}	Motor input Voltage
V_{mec}	Motor-ESC combo voltage input
V_s	Signal voltage
V_{shunt}	Voltage across shunt resistor
W	Watts
w_R	Error in calculated quantity
w_x	Error in measured quantity
x	Measured quantity

CHAPTER 1

1. INTRODUCTION

1.1. Background

The twenty-first century has seen a tremendous push towards electric vehicles, from cars to aircraft. This trend has been especially popular in the unmanned aerial vehicle (UAV) sector, due to the lower operating costs, reliability, and increased safety over their gas-powered counterparts. The surge in popularity has been the most evident for small UAVs weighing between 1-4 lbs. or 0.4-2 kg which are being used for research, search and rescue, agricultural survey, etc.

With this rise in popularity of electric UAVs, the propulsion system at the heart of these vehicles have been of great interest. They usually consist of four components – a battery as the power source, an electronic speed controller (ESC) as a throttle, an electric motor to provide mechanical power, and the propeller that converts the mechanical power to thrust. Since all these systems are important, performance data is required to design a well-matched system.

1.2. Importance of propulsion system performance data

During the conceptual design of an aircraft, the weight and general configuration is known, and this can be used to estimate the thrust required from the propulsion system [1]. However, the thrust produced by the propeller will be a function of every other system component. It will depend on the motor's ability to spin the propeller fast enough, which in-turn will depend on the output from the battery.

Hence, to design a well-matched propulsion system that works at its optimal point, the engineer needs to know the performance of at least the battery, motor, and propeller. Moreover, it is often wrongly assumed that the ESC, which acts like a throttle valve in an Internal Combustion Engine, does not affect the performance as much as the other components.

1.3. Existing techniques and problems

The battery performance can easily be tested using many commercially available instruments. Robust, peer reviewed techniques are available to test the propeller performance. However, there exists no reliable technique to test the electric motors and the ESC. Even though dynamometers are available for testing big electric motors, they are not designed to test the sub-750 W motors that are generally used in small UAVs. Hence, in most cases, unless a motor is custom made for a purpose, the manufacturer is the sole source of information about the performance. This leads to propulsion systems being designed with assumed efficiency values for the motor, or with unreliable data.

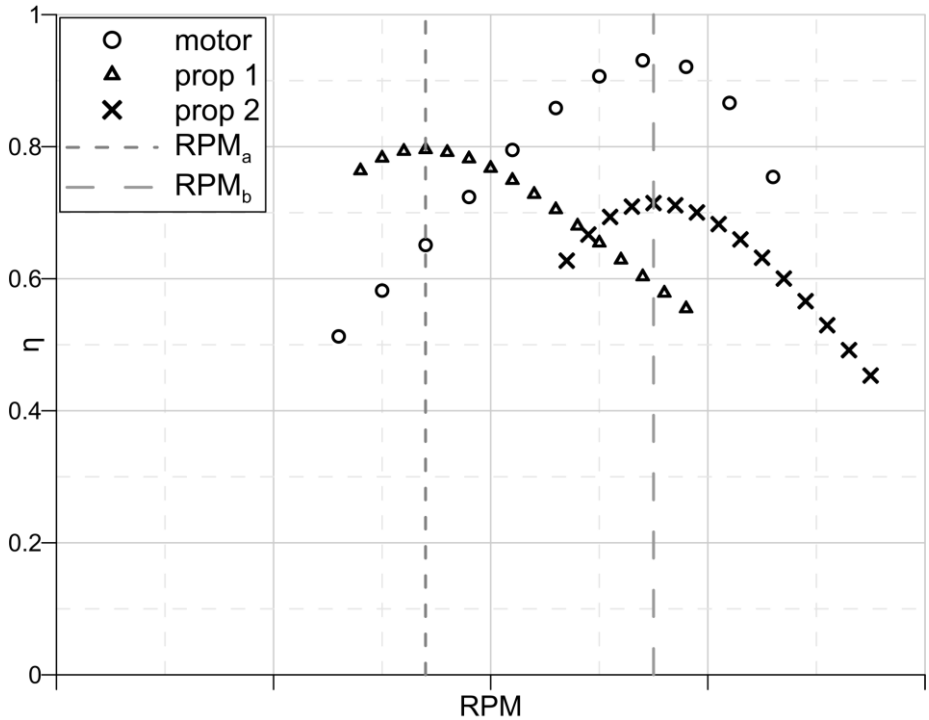

Figure 1. An illustrative efficiency curve for an electric motor overlaid with two illustrative propeller efficiency curves.

Figure 1 illustrates a general motor efficiency curve, along with two propeller performance curves as a function of the operational RPM (Revolutions per minute). These are not actual curves for any specific motor or propellers (props), but they highlight the importance of data for designers. Assume that the designer wants the prop to operate at its peak efficiency. From Figure 1, prop 1 clearly has a higher peak efficiency at RPM_a, compared to prop 2 at RPM_b. Now, if the motor can sustain both the props at their respective peak efficiency $RPMs$, the designer would assume that prop 1 will provide better system efficiency. However, combining the motor efficiency curve with the propeller efficiency, we see that, at their respective peak efficiencies, prop 1 will result in a system efficiency of approximately 52%, while prop 2 will result in an approximately 67% system efficiency. Hence, without reliable motor data, the predicted system performance

could be notably off. This could lead to reduced range, endurance, maneuvering capabilities, excessive current draw, etc. Another case that could arise is the motor not being able to produce the torque required to sustain the required RPM, resulting in the propeller operating at a different point.

1.4. Goals

Hence, there is a need to test electric motors to obtain necessary performance data for effective UAV design. The problem needs to be approached from an aircraft design perspective, with the necessary system variables identified. Secondly, a reliable, robust apparatus needs to be designed to measure these system variables. Third, the apparatus needs to be built and its proper operation ensured.

This thesis discusses the details that went into the design, building and testing of a small propulsion dynamometer. It also demonstrates how the obtained data can be used in conjunction with other propulsion system data to characterize the full system and to identify an optimal propulsion system for a UAV design. The system was mainly designed to test brushless out-runner motors. However, it can also test other types of motors with very little modification in the test procedure.

CHAPTER 2

2. THEORY

The problem is approached from an aircraft design perspective. A typical UAV design process is followed to understand the available data and find the gaps. To understand the thought process, we need to understand the working of the various components of an electric propulsion system. This chapter briefly talks about the theory behind operation and selection of all the components. This should help visualize the process involved and show how the apparatus design was conducted. However, this section is not meant to be an independent reference for propulsion selection.

2.1. Conceptual design routine

Generally during the aircraft conceptual design, thrust requirement plots for different flight phases are produced, as shown in Anderson [1]. They provide the minimum required thrust to meet the design requirements. Hence the required thrust from the propulsion system can be determined from these plots. Knowing the required thrust, the different propulsion system components can be selected as detailed below.

2.2. The battery

The selection of batteries will depend on a variety of factors like customer requirements, weight, technological restrictions, cost, range, endurance, required voltage and current. The usual design technique for UAVs is to select the battery chemistry first. Once the chemistry is selected, and abiding by voltage restrictions, the number of cells in the battery pack can be identified. Once the batteries are narrowed down, their performance can be evaluated using a battery analyzer like the one shown in Figure 2 to

obtain a time history of the battery voltage (V_{batt}) when drawing different fixed currents (I_{batt}), as shown in Figure 3.

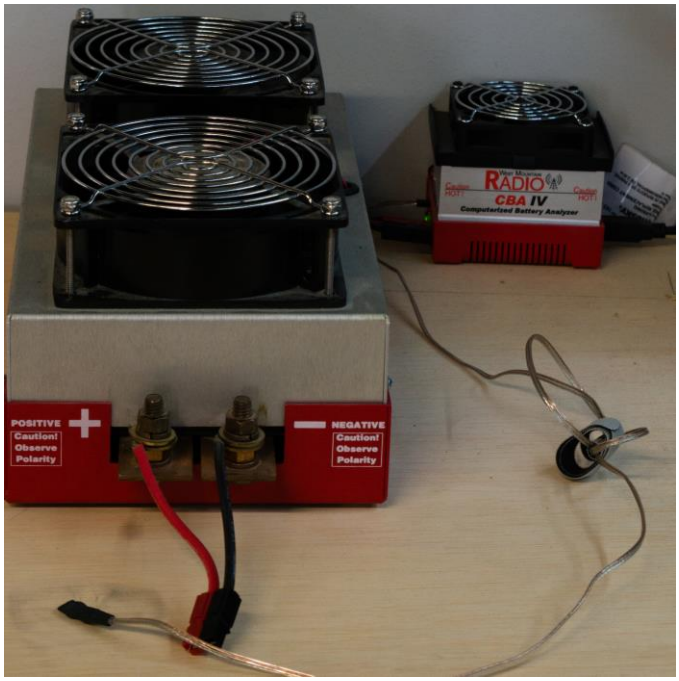

Figure 2. Battery testing apparatus used at Wichita State University.

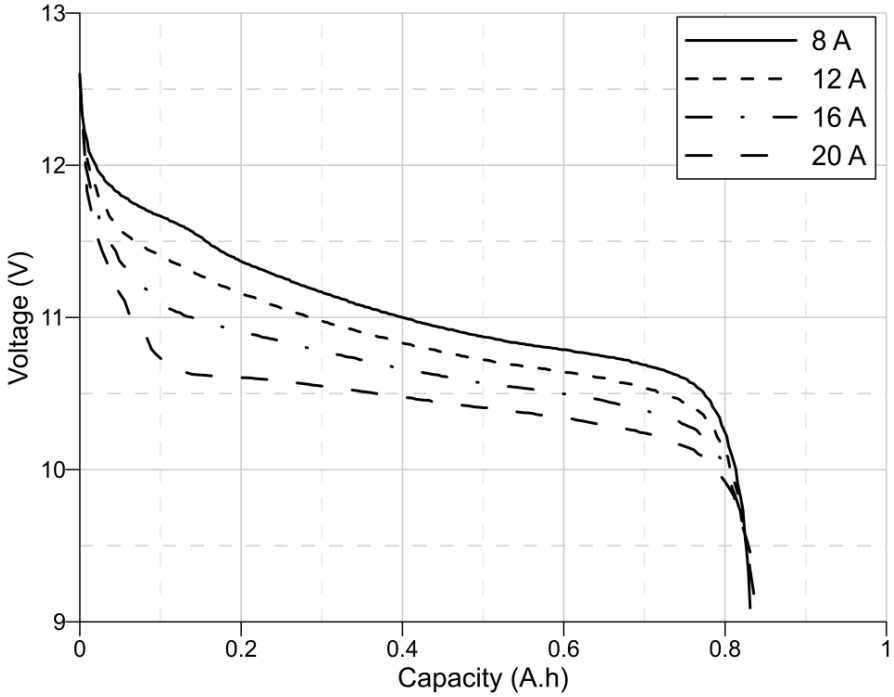

Figure 3. Performance history of *Great Planes Electrifly 3S 850 mAh* LiPo battery.

2.3. The propeller

If the choice of propellers is not restricted, historical trends in design can be used to narrow down the propeller size and type. This can be used as a starting point and the rest can be determined from requirements like cruise or top speed, ground clearance and specific mission requirements.

Merchant [2] details the technique used at WSU for propeller testing. The test output is presented in the form of Propeller Efficiency (η_p), Thrust Coefficient (C_{T_p}), Power Coefficient (C_{P_p}) and Torque Coefficient (C_{Q_p}) vs the advance ratio (J) as shown in Figure 4. Note that C_{P_p} represents the power required from the motor to spin the propeller, and not the power generated by the propeller. The above variables are calculated using equations (1) through (6), where T_p is the thrust produced by the propeller, Q_p the torque required from the motor, ρ the air density, n is the revolutions per second, D is the propeller diameter, P_p the power required to spin the propeller, Ω_p the angular velocity of the propeller, which is representative of the propeller RPM (RPM_p), and U the free stream velocity.

$$C_{T_p} = \frac{T_p}{\rho.n^2.D^4} \tag{1}$$

$$C_{Q_p} = \frac{Q_p}{\rho.n^2.D^5} \tag{2}$$

$$P_p = \Omega_p.Q_p \tag{3}$$

$$C_{P_p} = \frac{P_p}{\rho.n^3.D^5} \tag{4}$$

$$J = \frac{U}{n.D} \tag{5}$$

$$\eta_p = \mathrm{J}.\left(\frac{C_{T_p}}{C_{P_p}}\right) \tag{6}$$

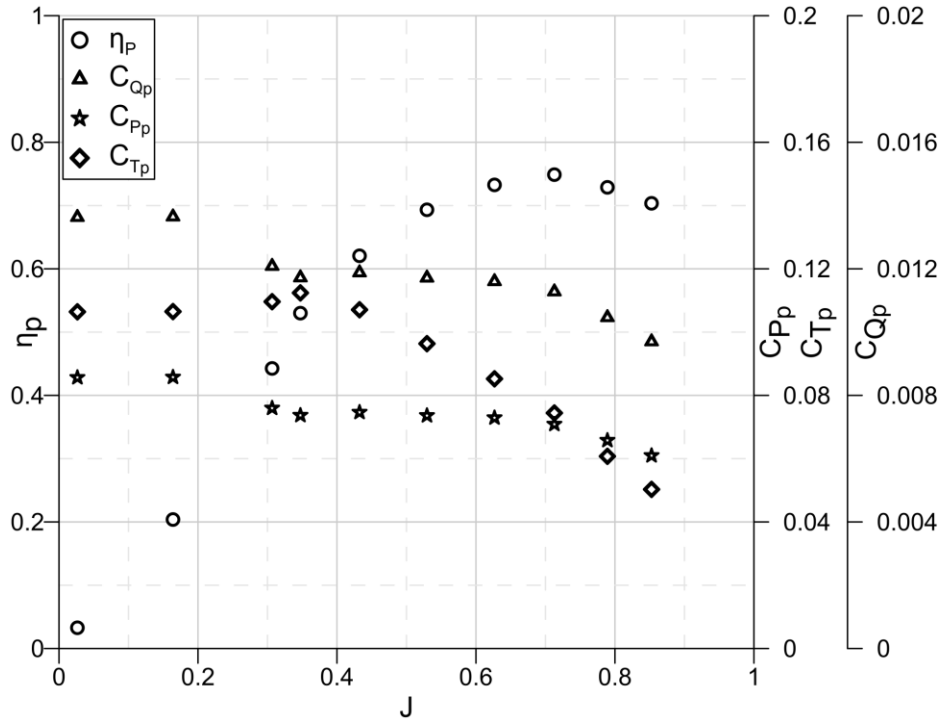

Figure 4. Performance data for an EAPC 12x12 propeller. This propeller has a diameter of 12” and pitch of 12”.

The propeller performance data can be converted into the form of T_p, Q_p, P_p, and η_p vs RPM_p at a specific flight speed (free stream velocity). Figure 5 gives T_p and η_p as a function of RPM_p along with Q_p required to spin the propeller at that RPM. In other words, we know the torque that the motor needs to produce, to maintain the RPM required for the prop to generate the required thrust, along with the efficiency at which the prop operates at that point.

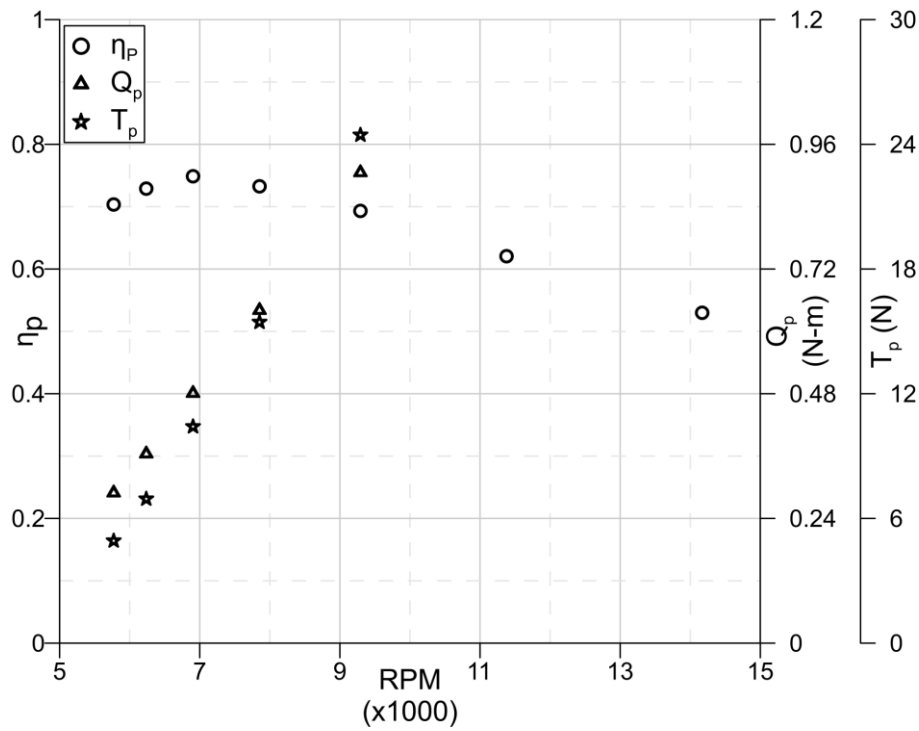

Figure 5. Dimensionalized performance data for the EAPC 12x12 propeller at $\rho = 1.225\ kg.m^{-3}$ and $U = 15\ m.s^{-1}$.

2.4. The motor

2.4.1. Types of electric motors

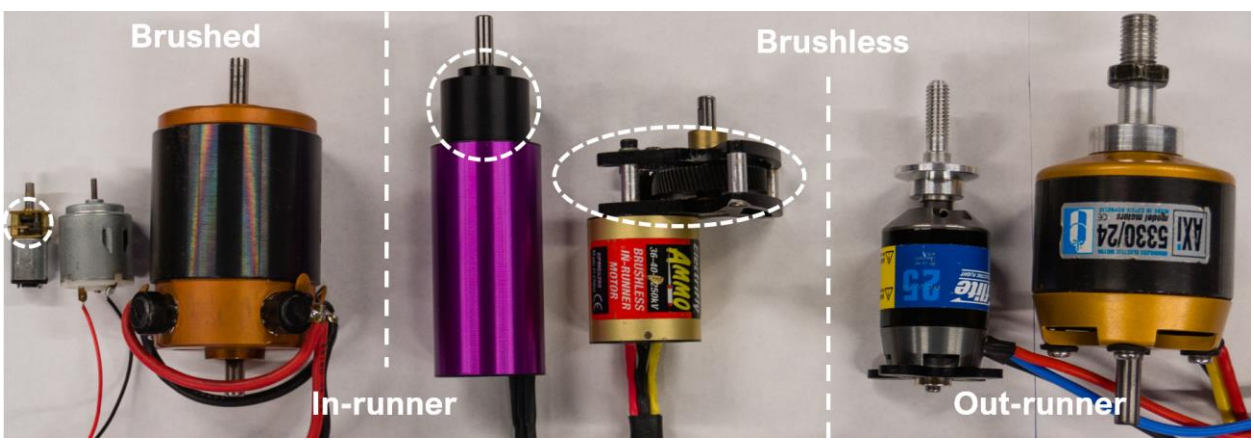

Figure 6. Various types of DC electric motors. The ovals mark gear-boxes.

DC Electric motors can be widely classified into brushed and brushless designs depending on the rotor configuration [3]. In brushed motors, the electric winding spins,

forming the rotor, within a constant magnetic field produced by the permanent magnets. Since the electric windings are spinning, fixed brushes are used to maintain current flow within the rotor. As the rotor spins, alternate windings get magnetized by the brushes and thus keeps it spinning. Moreover, the motor speed can be controlled by changing the applied voltage. However, the brushes wear due to friction. They also produce heat, which reduces the overall motor efficiency. Hence, these motors have a lower power-to-weight ratio compared to brushless motors.

Brushless DC motors keep the electric windings stationary, with the permanent magnets acting as the rotor. They do not need brushes to maintain electric contact, which makes them more efficient. However, since the windings do not alternate naturally, an external device needs to be used to alternately magnetize and demagnetize the stator coils, to spin the motor. This is done by the ESC which produces a carefully phased, switching DC signal.

Moreover, depending on the rotor position, the motors can also be classified into in-runner and out-runner motors, with most brushed motors designs being the former. In a brushless in-runner motor, the permanent magnet rotor is placed at the motor core. Thus, these motors can spin at very high RPM. However, with a very low rotor diameter, they have low torque and cannot spin all propellers. This can be compensated with gear systems which increase the torque output and decreases the output RPM, thus making them suitable for some UAV propulsion applications.

Finally, out-runner motors are generally only brushless. They use the outer casing or motor bell as the rotor. With the higher rotor diameter, they can produce higher torque

compared to in-runner motors. Moreover, since the higher torque is achieved without any gearing, they are more reliable and can cost less than a geared in-runner motor. They can also sustain crashes a lot better than geared in-runners, which makes them popular for UAVs. They also do not lose any efficiency from gear related losses.

2.4.2. Motor model

The motor model presented in AstroFlight, Inc.'s Electric Motor Handbook by Boucher [4] is used. All electric motors convert electric power (P_{in_m}) to mechanical power (P_{out_m}) as defined by equations (7) and (8), where V_{in_m} is the voltage applied to the motor, I_{in_m} the current drawn by the motor, Ω_m the angular velocity of the motor shaft and Q_m the torque at the shaft. Thus, we can define the motor efficiency (η_m) using equation (9).

$$P_{in_m} = V_{in_m}.I_{in_m} \tag{7}$$

$$P_{out_m} = \Omega_m.Q_m \tag{8}$$

$$\eta_m = \frac{P_{out}}{P_{in}} = \frac{\Omega_m.Q_m}{V_{in_m}.I_{in_m}} \tag{9}$$

Some other important variables for an electric motor are the speed constant (K_v) with units RPM/V, the torque constant (K_t) with units $N\text{-}m/A$, the motor resistance (R_m), and the current at zero load (I_0). Equations (10) through (12) show how they relate to the motor input and output. For an ideal motor with no losses, R and I_0 are zero and hence equations (13) and (14) apply.

$$RPM_m = K_v.(V_{in_m} - I_{in_m}.R_m) \tag{10}$$

$$\Omega_m = 2.\pi.RPM_m/60 \tag{11}$$

$$Q_m = K_t.(I_{in_m} - I_0) \tag{12}$$

$$RPM_{m_{ideal}} = K_v.V_{in_m} \tag{13}$$

$$Q_{m_{ideal}} = K_t . I_{in_m} \tag{14}$$

The K_v of a motor is almost always specified by the manufacturer. It is a good reference to compare the RPM capability of the motor, at a fixed voltage. Also, from equations (10) through (12), we can infer that when no load is applied to the motor, i.e. for $Q_m = 0$, and $I_{in} = I_0$, the RPM_m will be at its maximum of $RPM_m = K_v.(V_{in_m} - I_0.R_m)/60$. As Q_m is increased by applying a load at the motor shaft, I_{in_m} will increase and hence RPM_m will decrease slightly, depending on R_m. Thus the RPM_m vs Q_m curve will have a negative slope, and the RPM_m vs I_{in_m}curve will have a positive slope. Moreover, from Sections 2.2 and 2.4, we know that V_{batt}, I_{batt}, RPM_p, and Q_p are known. Knowing these, we can present the motor data in the form of η_m, Q_m, P_{out_m}, and I_{in_m} as functions of RPM_m, for a fixed V_{in_m}. This data can be acquired at different input voltages.

Every motor also has a maximum current (I_{max}) and power (P_{max}) that it can sustain. These are usually specified by the manufacturer. In case they are not specified, the parameter can be calculated from the specified one using equation (7). However, the P_{max} is specified at the maximum design voltage. If the V_m used is lower, the P_{max} will be lower and needs to be calculated using I_{max} and the current V_m.

2.5. The electronic speed controller

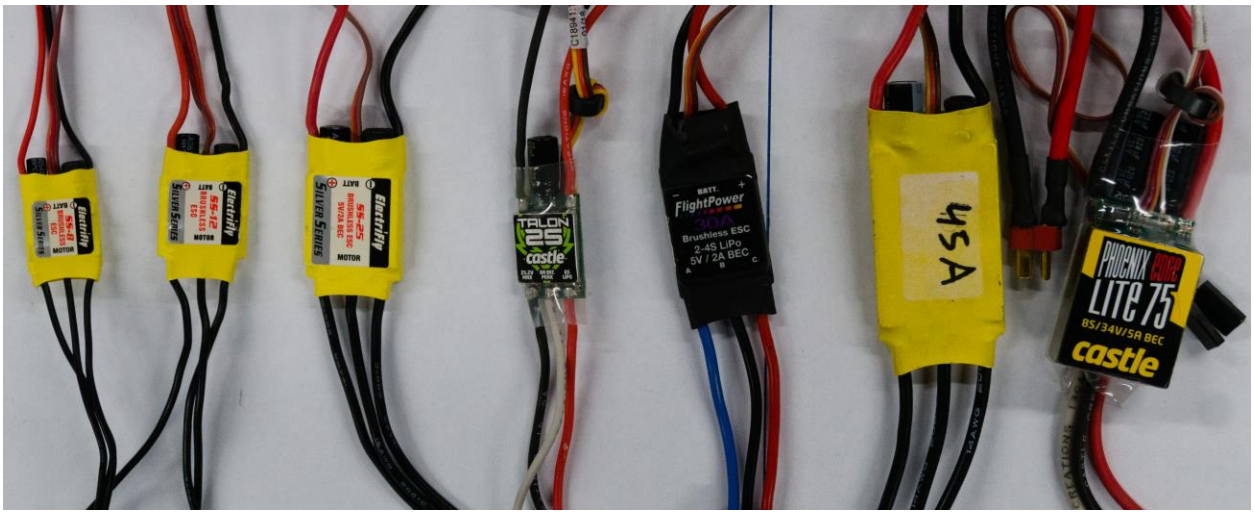

Figure 7. Brushless ESCs of varying current ratings. From left to right: 8A, 12A, 25A, 25A, 30A, 45A, and 75A.

All electric motors need a speed controller to act as a throttle. However, speed controllers for different types of motors function differently [5]. Brushless ESCs use Metal-Oxide-Semiconductor Field-Effect-Transistors (MOSFETs) [6], which act as switches, and use a Pulse Width Modulated (PWM) signal input for throttle. The MOSFETs are turned ON and OFF at varying frequencies to change the net voltage seen by the motor. ESCs also have Back-EMF (Electromagnetic field) sensors built-in to sense the motor rotation direction. Because of the switching required to spin the motor, brushless ESC output a phased switching DC, which alternates between the three motor stator windings. Figure 7 shows a few brushless ESCs.

Modern MOSFETs are highly efficient. However, they still can cause losses that affect the overall efficiency. We will test the combined performance of the ESC and the motor. This does not change the motor performance, as brushless motors cannot work without a brushless ESC, and the motor data can be collected with the specific ESC to be

used with it. Hence from here on, the Voltage and Current at the ESC input terminals will be referred to as V_{mec} and I_{mec} and the motor-ESC efficiency will be referred to as η_{mec}, and this will be used to evaluate system performance. Note that mec stands for motor-ESC combo.

2.6. The system

As stated earlier, the propulsion system consists of a battery, ESC, electric motor and propeller. The battery performance is available in the form of time history of V_{batt} for a specific I_{batt} draw. The motor-ESC combo input V_{mec} and I_{mec}, and output Q_m and RPM_m. Finally, the propeller produces T_p at a given RPM_p and requires Q_p to maintain that. Knowing this, we can combine the data for the propeller and the mec to obtain the overall efficiency using equation (15). Comparing P_p with P_m, we can obtain the RPM at which the propeller will spin on a given motor-ESC combo. For that RPM, the η_p, η_{mec}, and I_{mec} can be predicted. Conversely, knowing the required thrust for the UAV and with a few propellers selected, we can check if the motor can obtain that thrust, and find the system efficiency at that thrust. The current draw can then be used to evaluate if the selected battery is sufficient for the purpose.

$$\eta_{sys} = \eta_{mec} . \eta_p \tag{15}$$

CHAPTER 3

3. TEST APPARATUS

3.1. Apparatus concept

From section 2.4. we know that the motor efficiency is the ratio of the output and input powers. These in turn are quantified using Q_m and RPM_m, and V_{mec} and I_{mec}, respectively. To obtain the mec performance, a test is run at a constant voltage (V_{mec}) and constant 100% throttle level. Q_m and RPM_m are then varied, and I_{mec} monitored to identify the motor-ESC combo efficiency.

The torque, Q_m, is set by changing the load on the motor shaft. The higher the load applied at the shaft, higher the torque extracted from the motor. Physically, this load provides resistance against the motor rotation. It could be something as simple as a pair of pliers clamping down on the shaft or a brake system slowing down the rotation. Hence, to test a motor, we need a technique to apply a load at the motor shaft and to measure Q_m, RPM_m, V_{mec}, and I_{mec}.

3.2. Apparatus overview

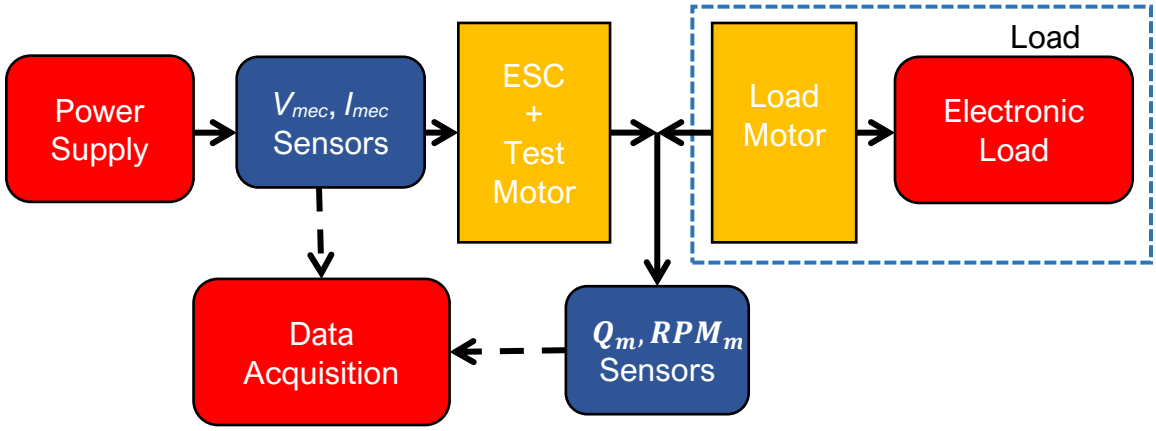

Figure 8. Overview of the motor test apparatus.

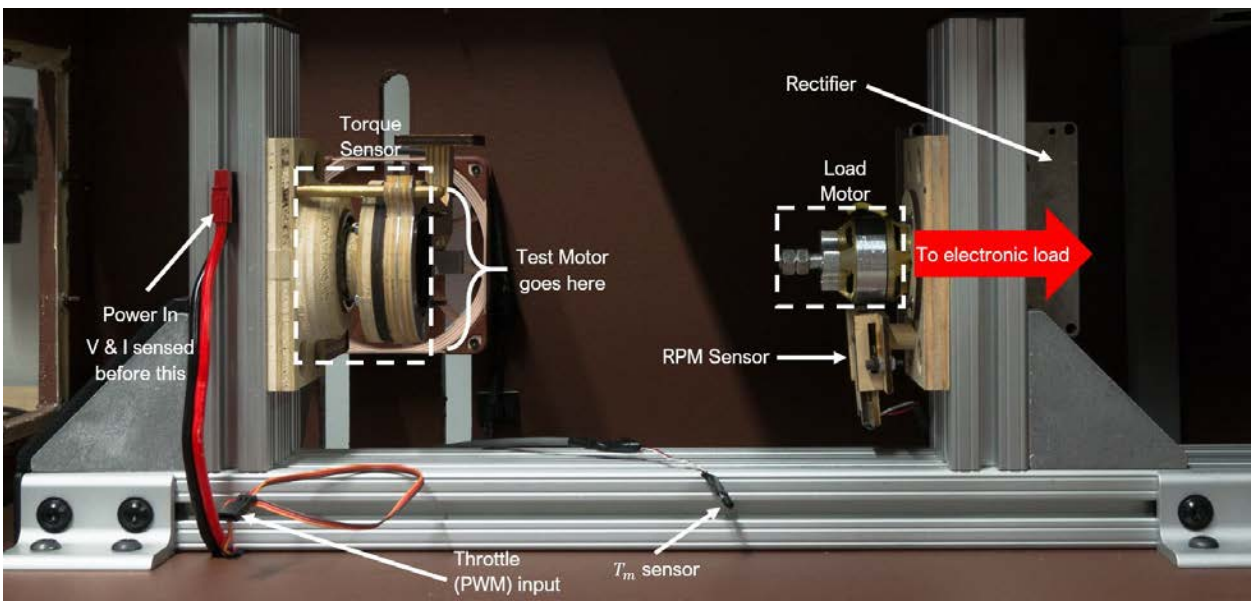

Figure 9. The test section and its various components.

Figure 8 gives an overview of the apparatus designed for this thesis. The test motor is powered by a programmable DC power supply, which provides a constant voltage and sufficient current to run the motor. The input current and voltage applied to the ESC input terminals are sensed. The load required is produced by a load motor constituted by a DC brushless motor connected to a programmable resistive electronic load. When the load

motor shaft is connected to the test motor shaft, it operates as an electrical generator producing current. The electronic load resists this current, producing a physical load at the link between the motors. This method was chosen over many other load designs to provide a predictable, controllable and calibrated load that is independent of other external factors like friction, temperature, etc., that is characteristic of a brake type system. Since the load motor is brushless, the output current will alternate between the three poles, producing a switching DC. This is sent to a bridge rectifier which combines them into a single-phase DC. The quality of DC from the rectifier is not of concern as it does not affect the load performance, with the DC electronic load sinking a constant electrical power.

3.3. Power supply and electronic load

Figure 10. The power supply (top) and the electronic load (bottom).

A BK Precision 9115 Multi-Range Programmable DC Power Supply is used to power the test motor. It can supply up to 1200 W with 0-80 V potential difference and 0-

60 A current. This was chosen to provide a suitable controllable, and accurate input power with low noise. It also has a programmable power cutoff system, which is used to prevent damage to the test motor.

A BK Precision 8610 Programmable DC Electronic Load is used as the sink for the load motor. It can sink up to 750 W and can sustain up to 120 V and 120 A. This device can absorb a constant electric power, independent of the voltage appearing across it or the current flowing into it or drain a constant current independent of the voltage appearing across it, as long as the above limits are not exceeded. Moreover, this equipment also has built in mechanisms to eliminate temperature dependency. Hence it provides a very reliable way to produce a test load. Through testing, it was found that the constant current mode provided the most control, allowing the user to perform a smooth torque sweep.

3.4. Sensors

3.4.1. Voltage sensor

The voltage divider circuit shown in Figure 11 is used to measure the voltage across the ESC input terminals. This circuit is connected via an opto-isolator to a 16-bit Analog-to-Digital Converter (ADC). The opto-isolator was added to prevent ground-loops.

From voltage divider theory [7], we know that the output analog signal (V_s) is defined by equation (16) which results in a linear analog behavior. A calibration was also done to ensure that the output is as expected.

$$V_s = V_{mc} \cdot \frac{R_2}{R_1 + R_2} = V_{mec} \cdot \frac{1k\Omega}{5k\Omega} \tag{16}$$

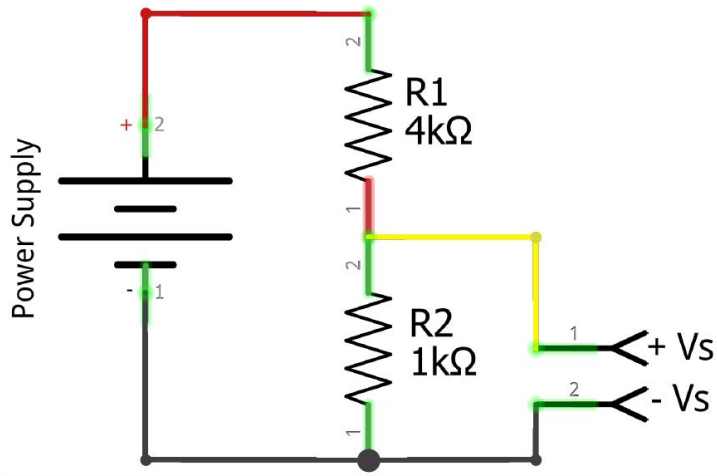

Figure 11. Schematic of the voltage divider circuit designed to measure V_{mec}.

3.4.2. Current sensor

The 'AttoPilot 90A Current Sensor' is used to sense the current through the system. It uses a 0.5 milli-Ohm shunt resistor and a Texas Instruments INA-169 chip to measure the current and output a 3.3V analog signal. This is connected to a 16-bit ADC via an opto-isolator.

The Attopilot also has a built-in voltage sensor. However, it was found to be extremely inaccurate and hence a switch was made to the custom voltage sensor discussed in Section 3.4.1.

3.4.3. Torque sensor

The torque is measured by mounting the test motor to a low friction roller bearing system as shown in Figure 12. When the motor shaft rotates, the reaction force makes the base rotate in the opposite direction with the same Torque (Q_m) as per Newton's Third Law of motion. This torque applied on the base is transferred via a moment arm of calibrated length (d) to a load cell which measures the tangential force (F_{LC}). Torque calculation is done using the definition of torque shown in equation (17). The load cell is

connected to the data acquisition using a HX711 24-bit load cell amplifier / ADC. The high-accuracy *10 Hz* data rate is used to collect the readings.

$$Q_m = F_{LC}.d \tag{17}$$

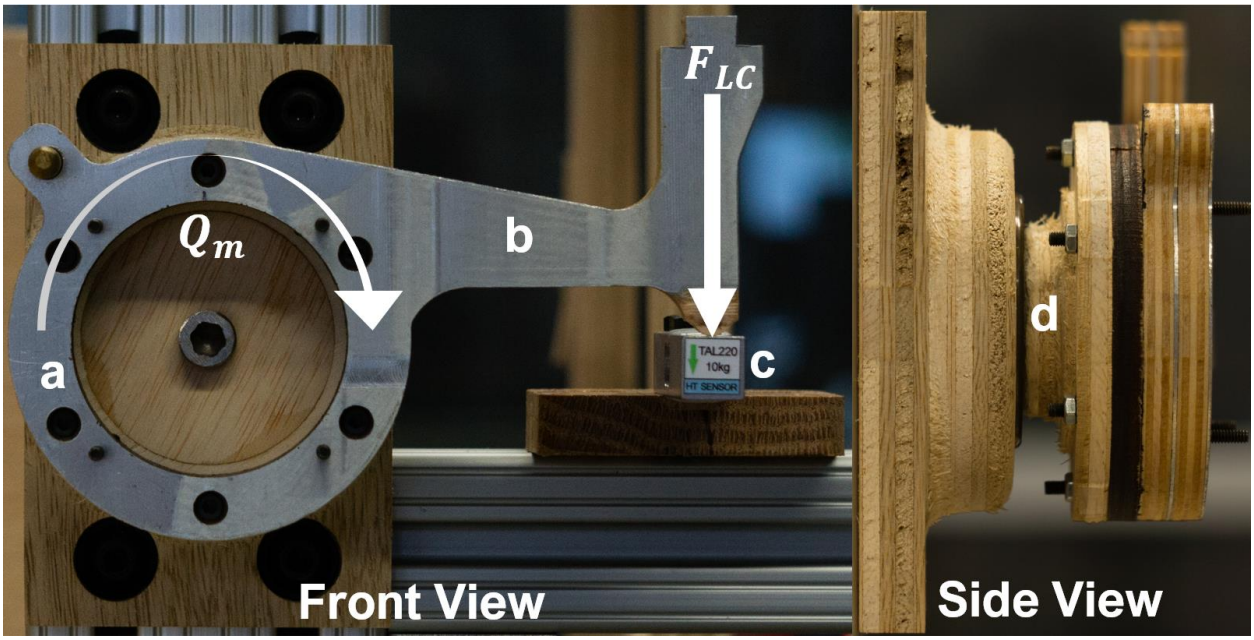

Figure 12. The system used to measure Q_m. a) motor mount; b) moment arm; c) load cell; d) roller bearing.

Figure 13. The bearing used in the torque sensor.

Figure 13 shows the SKF 3205 A/C3 Double Row Angular Contact bearing used in the torque sensor. It uses two rows of ball bearings set in a high tolerance channel to provide very low friction rotary motion while resisting off-axis movements. These figures are extracted from the CAD model provided by the manufacturer [8].

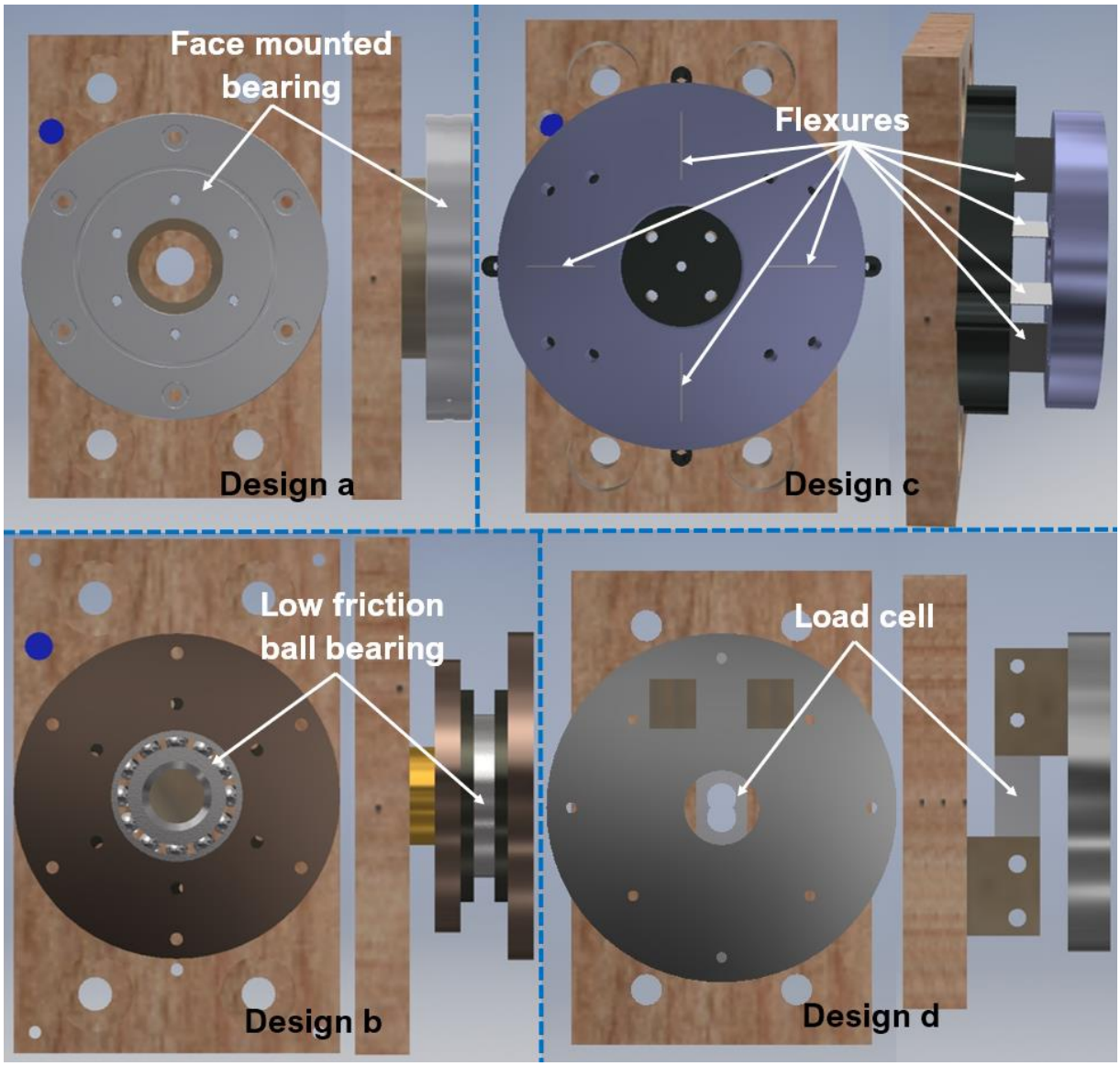

Figure 14. Some designs that were attempted to measure Q_m.

Figure 14 shows some other designs that were attempted and abandoned to measure Q_m. Designs a through c used the same principle as the final design, utilizing a

moment arm to transfer a tangential force to the load cell. However, they used different techniques to isolate the rotary motion. ‘Design a’ used a face mounted roller bearing, which completely isolated the rotary motion. However, it had high friction and locked up at times. ‘Design b’ used a low friction ball bearing system to isolate the rotary motion. However, the bearing was too compliant off the rotary axis, with the test motor capable of tilting off the rotary axis. This led to resonance tumbling of the motor. A similar design with two parallel ball bearings were attempted, to reduce the compliance. However, it was not enough, and the improvement was only marginal. ‘Design c’ used very thin flexures to isolate the torque effectively. However, it failed in operation due to fatigue on the extremely thin flexures, that were necessary to properly transfer the moment reliably. Finally, ‘design 4’ was supposed to directly utilize the flexing of the load cell to measure the torque. However, it was determined that this design did not transfer a force to the load cell, as predicted. A possible fix to design 4 will be discussed in the Recommendations section.

3.4.4. RPM sensor

An optical sensor as shown in Figure 15 is used to measure the *RPM*. The load motor bell is painted black (non-reflective) with a shiny (reflective) strip covering approximately half of its circumference. A reflective IR sensor, made up of a pair of IR emitter and detector, is used to sense the presence of the reflective stripe, as the motor spins in front of it. The sensor is paired with a very high frequency ADC capable of up to 3,300 samples/s and a custom software. The data acquisition system records the analog output from the IR sensor for approximately 1 s along, with the time at each data point. A

Schmitt Trigger is then applied using a suitable threshold to make a pseudo-digital signal, with a waveform with identifiable wave edges.

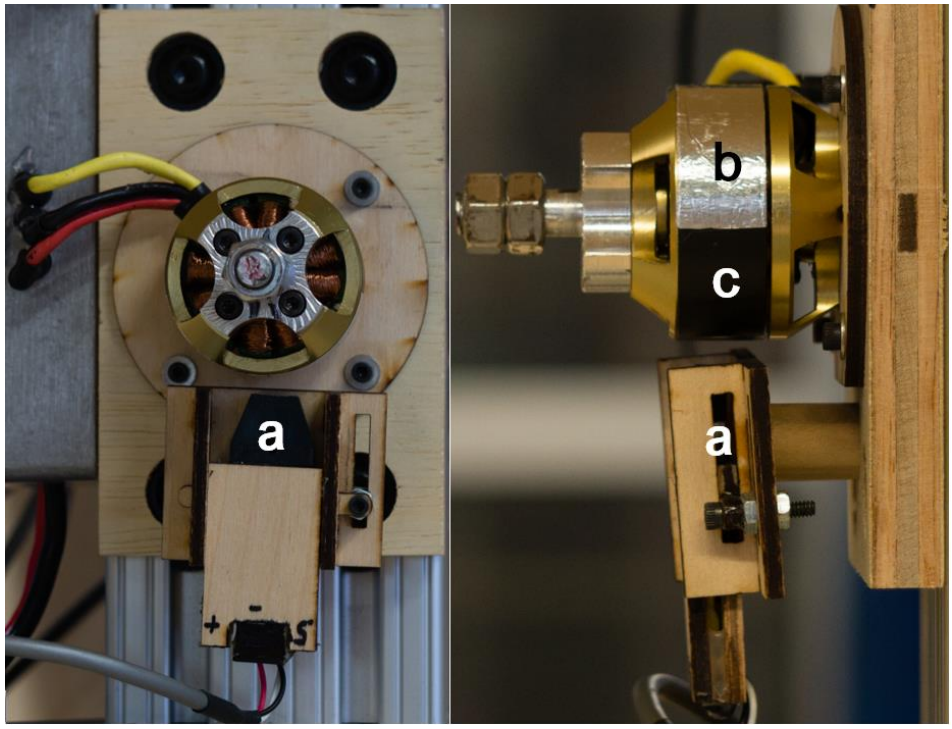

Figure 15. The RPM sensor setup along with the load motor. a) IR emitter + detector; b) reflective stripe; c) non-reflective stripe.

Figure 16 shows a signal from the RPM sensor, along with its corresponding pseudo-digital signal. The troughs and peaks correspond to the reflective and non-reflective sections, respectively. The rises in the pseudo-digital signal are found and the average time difference between them used to calculate the RPM and ω using equations (18) through (20). In testing it was found that the data acquisition limits the ADC read rate to approximately 900 samples/s, which makes this system capable of sensing anything up to approximately 27,000 *RPM*, which is sufficient for this application.

$$RPS = \left(t_{average_{rise}}\right)^{-1} = \left(t_{average_{fall}}\right)^{-1} \tag{18}$$

$$RPM = RPS.60 \tag{19}$$

$$\omega = 2.\pi.RPS \tag{20}$$

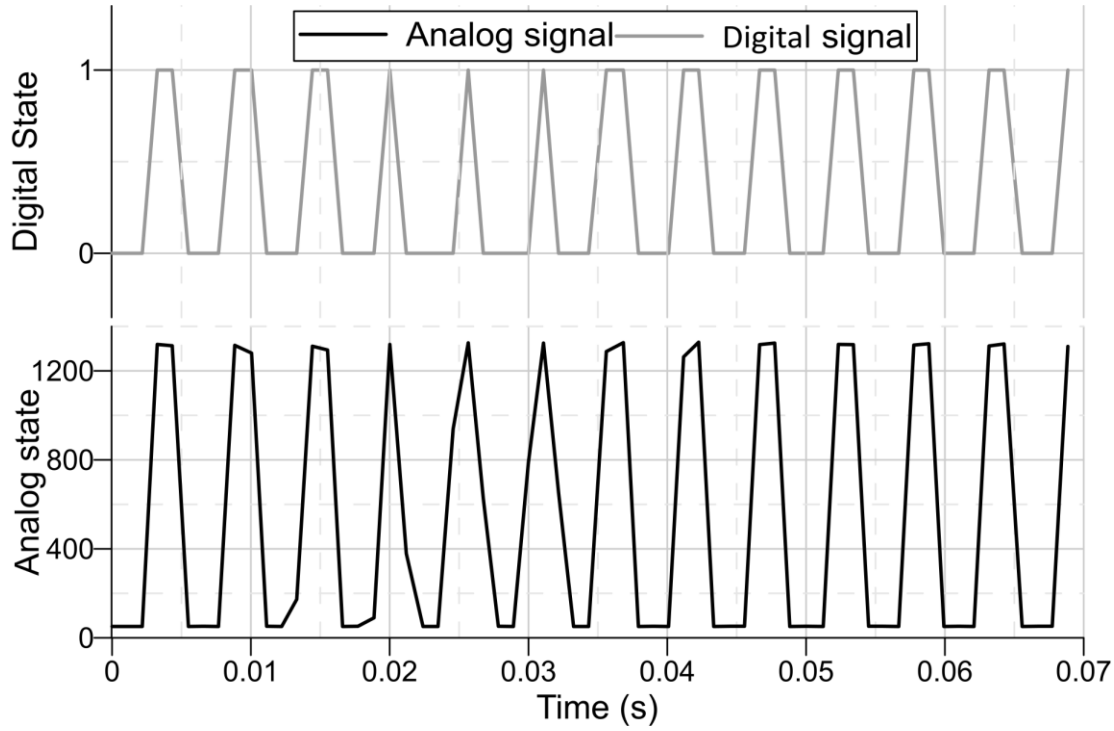

Figure 16. The signal from the RPM sensor, along with the pseudo-digital signal.

3.4.5. Temperature sensors

Two temperature sensors are used to monitor the room temperature (T_r), and the test motor temperature (T_m). The former is just for reference and the latter to understand how hot the motor could run when under load. The room temperature sensor is a MCP9809 High Accuracy Temperature sensor and the motor temperature sensor is a TMP36 thermistor.

3.5. Data acquisition

Data Acquisition is done on a Raspberry Pi 3. A 16-bit 860 Hz ADC is used to communicate to the voltage and current sensors and a 12-bit 3,300 Hz ADC is used to measure the *RPM*. Finally, the torque sensor is connected via a 24-bit 10 Hz ADC + amplifier. A one second sample period is used for the voltage, current and RPM sensors.

However, a five second sample period is used on the torque sensor to compensate for the lower sample frequency of the amplifier. Finally, a Python based GUI guides the user through the test procedure and manages all the sensor reads and test output.

3.6. Calibration

3.6.1. Voltage sensor

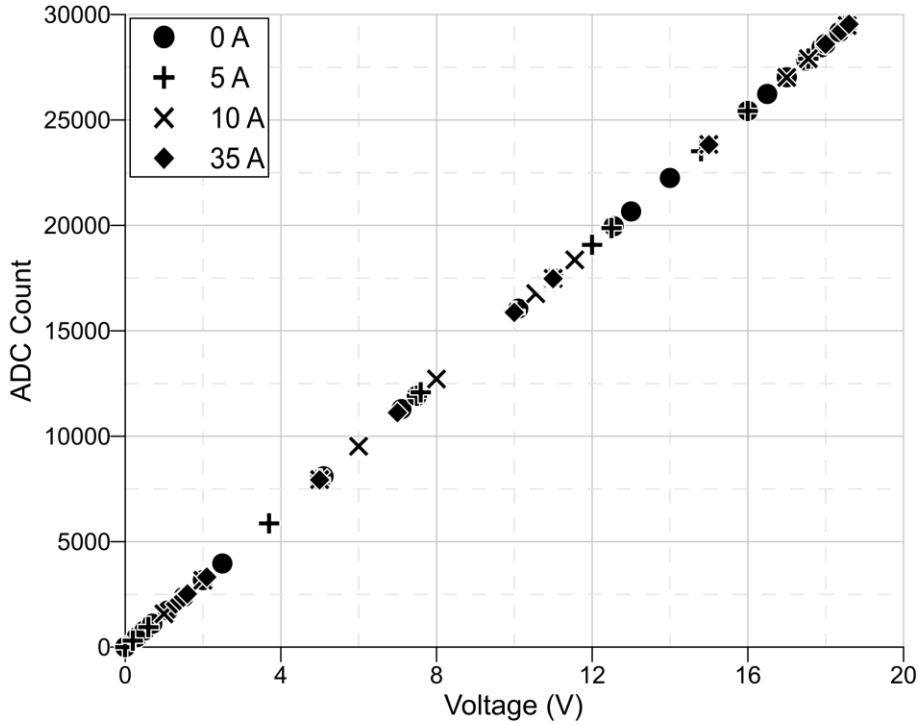

Figure 17. The calibration curve obtained for the voltage sensor. We see that the response is linear and independent of the circuit current.

The voltage sensor outputs an analog signal corresponding to the applied source voltage, which is converted by the ADC into a count reading. It was calibrated by recording the ADC count for varying supply voltage. This was done at three fixed currents to check for any current dependency. Figure 17 shows the calibration curve obtained for this sensor. We see that the sensor output is quite linear with minimal, if any, current

dependency. The sensor is viable till approximately 18.5 V, after which it causes ADC saturation, overloading the ADC.

3.6.2. Current sensor

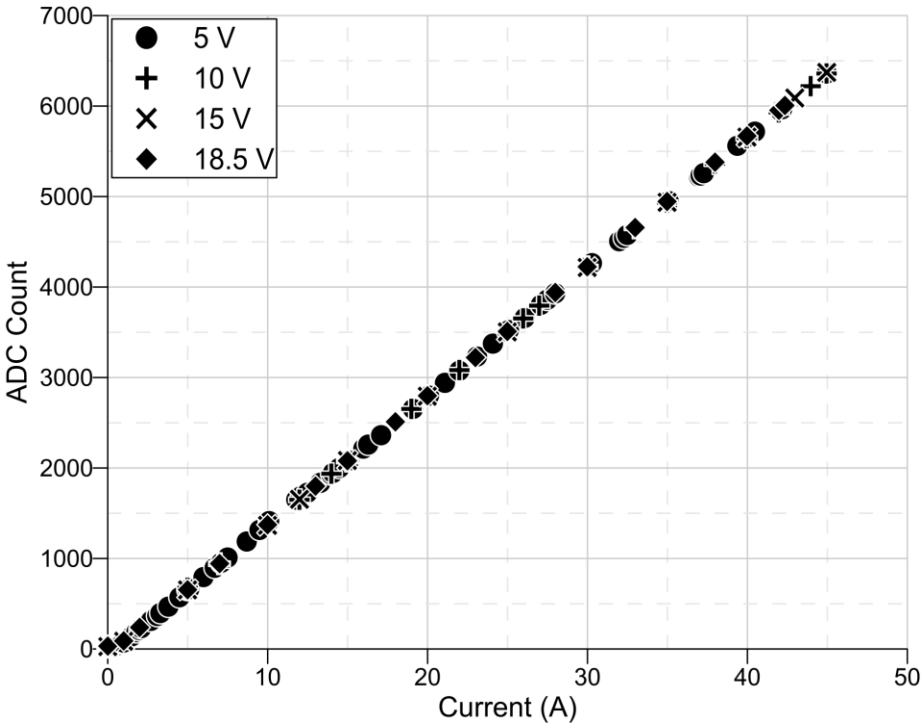

Figure 18. The calibration curve obtained for the current sensor. We see that the response is linear and independent of the voltage.

The current sensor outputs an analog signal corresponding to the detected current, which is converted by the ADC into a count reading. It was calibrated by connecting the power supply to the electronic load via the sensor. The voltage across the system (supply voltage) and the current flowing through it are controlled using the source and the load, respectively. The ADC count for each data point is recorded, and the calibration factor calculated. This was done for four different supply voltages to check for voltage dependency. Figure 18 shows the calibration curve obtained for this sensor. We see that the sensor output is quite linear with minimal, if any, voltage dependency. Close

inspection of the curve shows that the sensor is viable for currents greater than 1 A. This is however not of any concern as it does not affect the sensor's resolution, and this current is very low and well below the designed operating range. Finally, the system is calibrated only till 45 A which is the maximum rating of the physical connectors in the setup.

3.6.3. Torque sensor

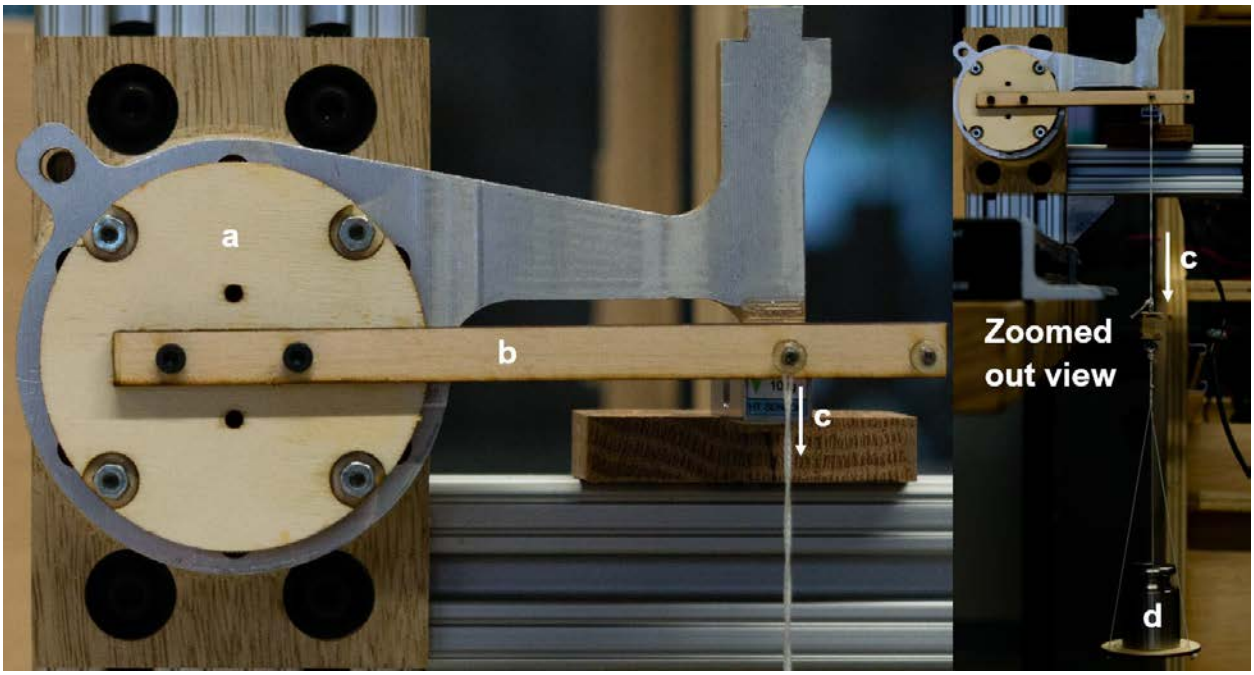

Figure 19. Torque calibration technique. a) Motor mount, b) caibrated moment arm, c) point force, d) calibrated weight.

From Section 3.4.3, we know that the torque is sensed by sensing the tangential force applied by a calibrated moment arm. The moment arm length was calibrated using a pair of Vernier calipers and obtained to be $0.10\,m$. With this known, only the force measurement at the load cell needs to be calibrated.

The HX 711 load cell amplifier and ADC, amplifies the signal from the load cell into a measurable voltage difference, sense this and produces a digital output corresponding

to the applied load. Hence the data acquisition reads an ADC count corresponding to the applied load.

Figure 19 shows the technique used to calibrate the torque. It uses a solid moment arm of calibrated length to which a force is applied. This system emulates the torque applied by the motor, by applying the torque to the motor mount and engaging the bearing. ANSI Class 7 calibration weights were used to apply a known force at the known distance, and the ADC count recorded. This is done up to a torque of *1 N-m* (*8.85 lb.-in*), which is well above the torque range from a small UAV motor. Moreover, the weights were varied in a random manner to sense any non-linear effects like elasticity or hysteresis in the load cell material, friction in the roller bearing, etc.

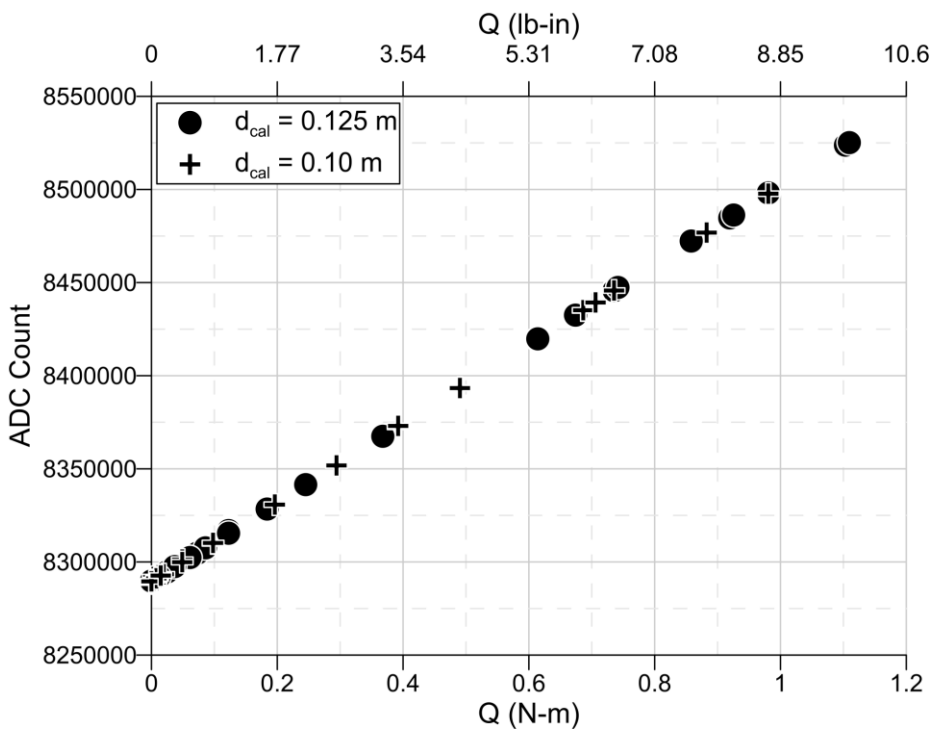

Figure 20. The calibration curve obtained for the torque sensor. We see that the response is linear, with no significant non-linear effecs.

Figure 20 shows the calibration curve for the torque sensor. We see that the curve is linear.

3.6.4. RPM sensor

The RPM sensor is in theory a ticker that registers when the shiny stripe passes over it. Hence, it doesn't need a calibration. It was however validated independently using an off-the shelf optical tachometer, a stroboscope and an oscilloscope.

3.6.5. Temperature sensors

The TMP36 thermistor outputs an analog voltage proportional to the sensed temperatures and do not require calibration. The MCP9809 room temperature sensor comes pre-calibrated.

3.7. Uncertainties and sensitivity analysis

Table 1 shows each of the expected sensor uncertainties. All the major sensors, i.e., Torque, RPM, V and I were calibrated experimentally. A known quantity was applied, and the sensed quantity compared with it. This was done multiple times and in random orders, to obtain a good sense of the errors. All uncertainties presented are local and are calculated using equation (21), except for the Torque Sensor Q_m, which is the Full-Scale Error calculated using equation (22). Moreover, all values are conservative.

$$Local\ Error = \frac{|Calibrated\ quantity - Sensed\ quantity|}{Sensed\ Quantity} \tag{21}$$

$$Full\ Scale\ Error = \frac{|Calibrated\ quantity - Sensed\ quantity|}{Maximum\ sensor\ capacity} \tag{22}$$

TABLE 1

THE MAXIMUM EXPECTED SENSOR UNCERTAINTIES.

Instrument	Measured Quantity	Maximum Expected Uncertainty	Unit
Voltage Sensor	V_{mec}	0.2	%
Current Sensor	I_{mec}	5	%
RPM Sensor	ω_m	2π	rad/s
Torque Sensor	Q_m	0.2	% FS
TMP36	T_m	±2	˚C
MCP9809	T_r	±0.25	˚C

Figure 21 shows the percentage full scale error in the torque measurement. We see that the uncertainties in the Q_m measurements would be less than 0.2% of the full-scale capacity, i.e. *1N-m* (*8.85 lb.-in*).

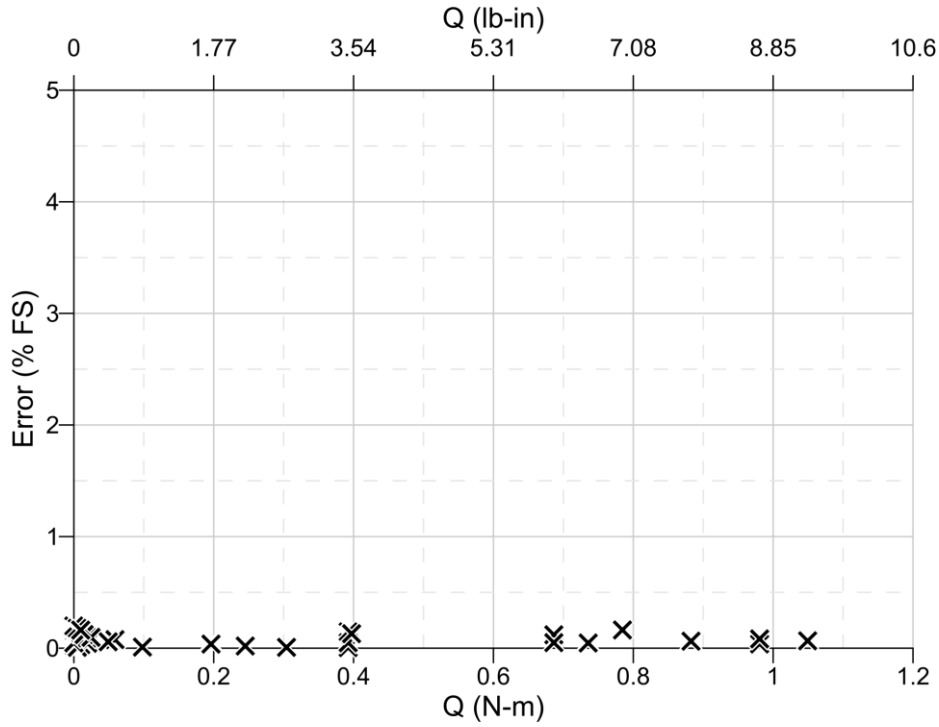

Figure 21. Percentage full scale error observed in the torque measurements.

Figure 22 shows the percentage error in the voltage measurement. We see that it has a maximum local error of 0.2%.

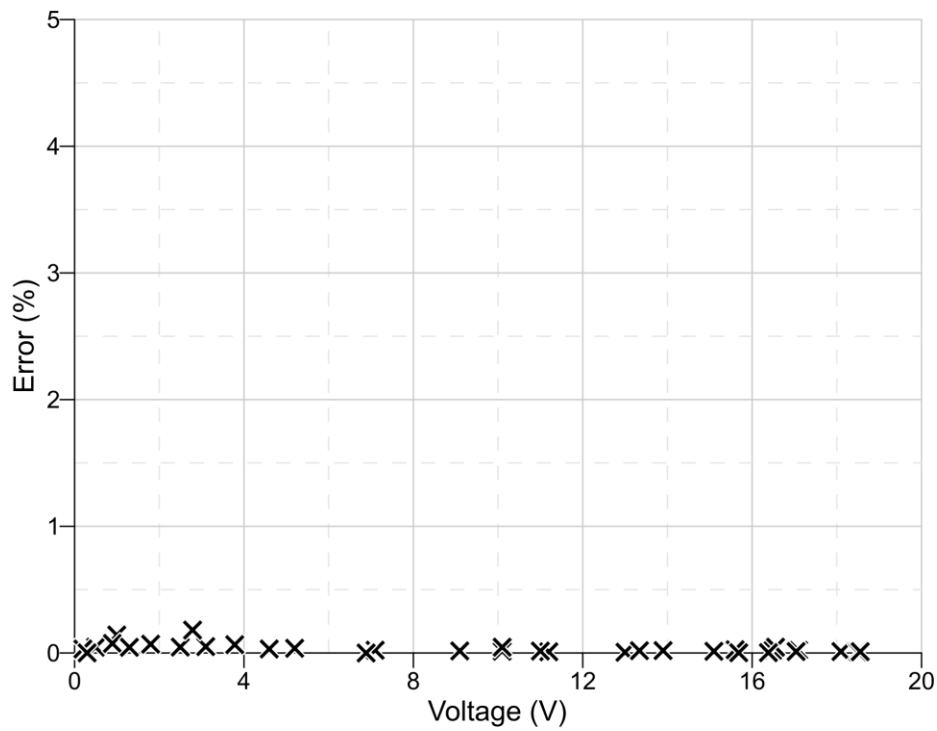

Figure 22. Percentage error observed in the voltage measurements. We observe errors less than 0.2%, across its range.

Figure 23 shows the percentage error in the current measurement. We see that the uncertainties in the I_{mec} measurements are less than 5% for currents from$1\ A$ to $5\ A$ and less than 0.75% above that. As mentioned in section 3.6.2, the current sensor is not viable for measurements under $1\ A$.

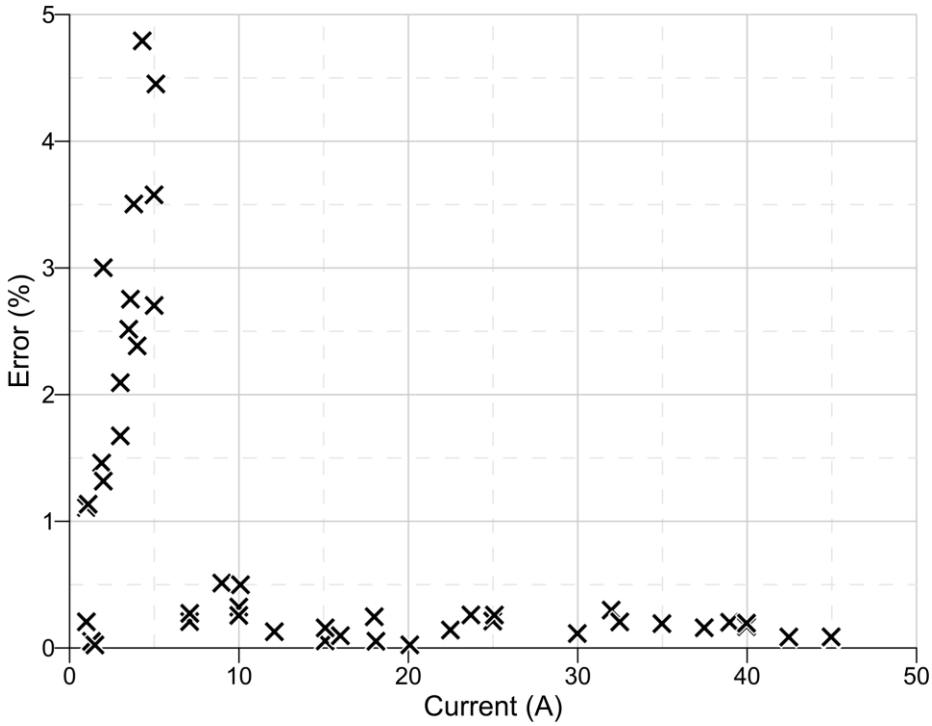

Figure 23. Percentage error observed in the current measurements. We observe errors less than 5% for low-current measurements and that below 1% for high-current measurements.

The uncertainty in the RPM sensor was found using an optical tachometer. It was found to have a conservative maximum uncertainty of ±1 RPS, corresponding to a $2\pi\ rad/s$ uncertainty in the Ω_m or $60\ RPM$, irrespective of the measured RPM.

The TMP36 thermistors used to monitor the motor temperature has a typical accuracy of $\pm 2\ ^{\circ}C$, in the expected operating range. Finally, the MCP9809 sensor used to monitor room temperature has a typical accuracy of $\pm 0.25\ ^{\circ}C$.

Knowing the uncertainties in the measured quantities, the uncertainties in the calculated quantities can be obtained using equation (23) as detailed in Wheeler and Gangi [9], where w_R is the expected uncertainty in a calculated quantity 'R' and x is a measured quantity used to calculate R.

$$w_R = \left(\sum_{i=1}^{n}\left[w_{x_i}.\frac{\partial R}{\partial x_i}\right]^2\right)^{\frac{1}{2}} \tag{23}$$

Equations (7) through (9) can be combined with equation (23) to obtain the errors in each of the calculated quantities, as shown in equations (24) through (26).

$$w_{P_{in_m}} = P_{in_m}.\left(\left(\frac{w_{V_{in_m}}}{V_{in_m}}\right)^2 + \left(\frac{w_{I_{in_m}}}{I_{in_m}}\right)^2\right)^{\frac{1}{2}} \tag{24}$$

$$w_{P_{out_m}} = P_{out_m}.\left(\left(\frac{w_{Q_m}}{Q_m}\right)^2 + \left(\frac{w_{\Omega_m}}{\Omega_m}\right)^2\right)^{\frac{1}{2}} \tag{25}$$

$$w_{\eta_m} = \eta_m.\left(\left(\frac{w_{V_{in_m}}}{V_{in_m}}\right)^2 + \left(\frac{w_{I_{in_m}}}{I_{in_m}}\right)^2 + \left(\frac{w_{Q_m}}{Q_m}\right)^2 + \left(\frac{w_{\Omega_m}}{\Omega_m}\right)^2\right)^{\frac{1}{2}} \tag{26}$$

3.8. Limitations

TABLE 2

THE LIMITATIONS OF THE MOTOR TEST STAND COMPONENTS.

Measured Quantity	Source	Operational range	Unit
$\boldsymbol{V_{mec}}$	ADC	$0 - 18.5$	*V*
$\boldsymbol{I_{mec}}$	Sensor/ wiring	$1 - 45$	*A*
$\boldsymbol{RPM_m}$	Data Acquisition	$27{,}000$	RPM
$\boldsymbol{Q_m}$	Sensor	1	*N-m*
$\boldsymbol{P_{out_m}}$	load	750	*W*

The various components and sensors of the setup have limitations, as discussed in their respective sections. Table 2 summarizes these limitations, that need to be

understood, to ensure safe operation of the system. We see that the maximum permissible voltage is $18.5\ V$, limited by the ADC. The maximum permissible current is $45\ A$ because of the electrical wirings used in the setup and the minimum that can be accurately measured is $1\ A$. The maximum RPM that can be reliably read by the data acquisition is $27{,}000\ RPM$. The maximum power that can be reliably read and sustained by the torque sensor is 1 *N-m* (*8.85 lb.-in*). Finally, the maximum power that can be sustained by the load is $750\ W$.

Note that the maximum RPM and power listed here are not the same as the maximum RPM and power that can be safely applied to the load motor, which will be discussed in the Test procedure section. Moreover, the test motor should never be operated above its maximum ratings, as will once again be discussed in the Test procedure section.

Operating at conditions outside those specified in Table 2 could result in unreliable data and or irreparable damage to the test motor, and the test apparatus. Operating at current and power ratings outside the limitations could also easily result in fire.

CHAPTER 4

4. PROCEDURE

4.1. Pre-test requirements

Before the motor can be tested, its designed operating conditions need to be known. Specifically, the voltage ranges it can be operated at, the maximum current allowable for the specific ESC-motor combination and its maximum power rating. Now, the desired test conditions can be selected. For example, if the motor is going to be operated with a *3S Li-Po* battery, it can be tested at $11.1V$, corresponding to the nominal voltage.

4.2. Test procedure

This section provides a brief testing procedure. A more detailed user manual is provided in the Appendix. A typical test procedure is as follows:

i) Test voltage, maximum current and power are determined;

ii) The test motor is mounted to the torque sensor;

iii) An appropriate load motor is mounted on the load side.

The load motor needs to be capable of sustaining the RPM and power produced by the test motor. It was experimentally determined that the load motor needs to be rated for approximately 2.2 times the power as the test motor. For example, to test a $300\ W$ motor, a $600\ W$ load motor needs to be used.

iv) The motors are linked together using sockets and a steel stock bar-link.

v) The torque system is tared.

vi) The power source is set up for the appropriate test conditions – constant voltage, maximum current and power.

It is extremely important that the user follow the I_{max} and P_{max} ratings as the motor could be irreparably damaged if operated at higher currents. It is always safer to set the maximum current a bit below the manufacturer recommendations and extrapolate the data.

vii) The electronic load is set to constant current sink mode starting at $0\ A$. The sink current is slowly increased, to increase the load on the test motor, decreasing its RPM.

viii) The RPM is very slowly decreased as described above, till the motor approaches its maximum current or power rating. The data points are collected at suitable RPM intervals in the desired range.

4.3. Test outputs

The data acquisition outputs a text file with the test points. For each test point, the V_{mec}, I_{mec}, Q_m, RPM_m, $P_{in_{mec}}$, P_{out_m}, η_{mec}, T_m, and T_r are printed. The calculated powers are provided in Watts as is characteristic with small electronic systems. However, the torque is provided in both *N-m* and *lb.-in*, for convenience aligning with common aircraft design practices in the United States. The output is formatted with '|' as delimiters, thus providing a format that can easily be visually scanned as well as imported into necessary software. Moreover, with the system outputting all necessary variables, the output needs very minimal post-processing, if any.

CHAPTER 5

5. RESULTS AND DISCUSSION

Figure 24. The test stand that incorporates all the required equipment.

Figure 24 shows the test stand that was designed and built. It incorporates the test apparatus, power supply, electronic load, and data acquisition into one unit that is convenient to use and store. Any brushless motor operating within the system's design parameters can be tested here.

A series of tests were run to ensure good data repeatability and to understand and prove the test stand operation. All maximum ratings used in these tests are the continuous

ratings specified by the manufacturer. In most cases the I_{max} and P_{max} are set slightly below the ratings to ensure a margin of safety. Also, all tests are run at 100% throttle, unless specified.

5.1. Repeatability

It is very important that the system produce repeatable data. Two pairs of motor-ESC combos are tested at similar conditions to ensure good data repeatability. Both pairs are tested thrice, and the results compared.

Figure 25 shows the performance data for the *Great Planes Rimfire 400* brushless out-runner motor with the *Castle Creations Talon 25A* ESC, tested at $11.0\ V$ with the I_{max} and P_{max} set to $13A$ and $143W$, respectively. The motor has a K_v of $950\ RPM/V$. It is designed to be operated in a $7.4\ V$ to $11.1\ V$ range and has an I_{max} and P_{max} of $14.4\ A$ and $160\ W$, respectively. Also, the ESC is designed to be used in a $7.4\ V$ to $25.2\ V$ range at a maximum of $25\ A$. We see that the three tests produce very similar results, with the P_{out_m}, Q_m, and I_{mec} data repeating extremely well in the full range. However, there is noticeable spread of approximately $6\ \%$ in η_{mec} at RPM_m greater than $9{,}000$. Even though, this spread can be interpreted as weak repeatability, we will see that this could just be a characteristic of this particular mec combo, as many other tests do not show any such issues.

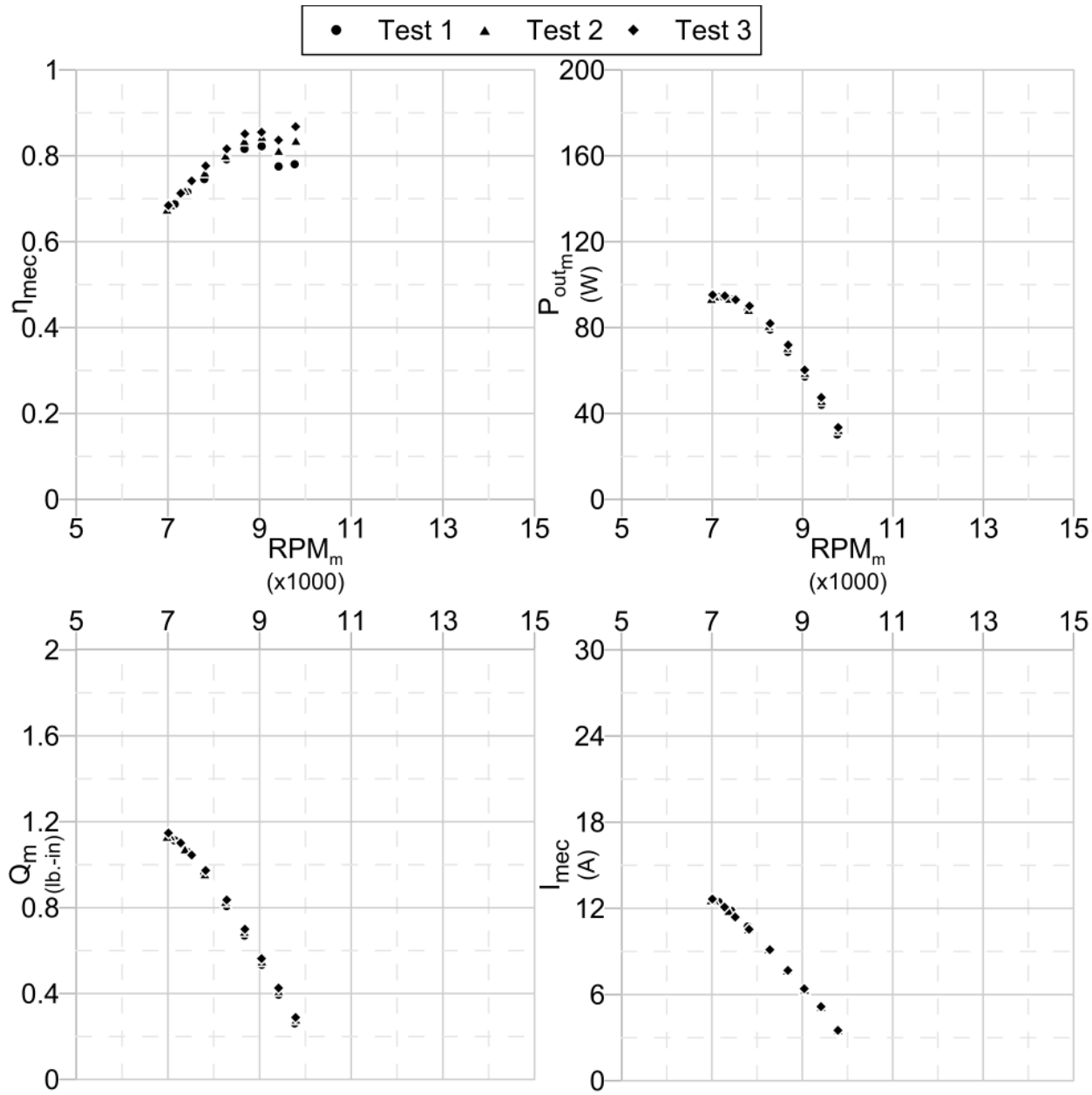

Figure 25. Performance data for the *Rimfire 400* with the *Talon 25A*, tested at $11.0\ V$.

Figure 26 shows the V_{mec} sensed by the voltage sensor during this test. With the power supply providing a very steady voltage, we see that the voltage sensor produces data that repeats extremely well.

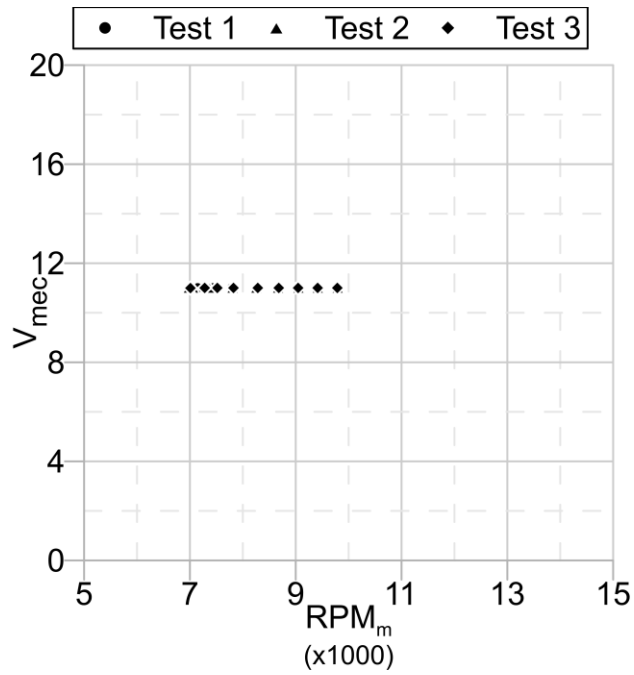

Figure 26. The sensed V_{mec} for the *Rimfire 400* with the *Talon 25A*, tested at $11.0\ V$.

Figure 27 shows the performance data for the *Scorpion SII-2212-1400KV* brushless out-runner motor with the *Great Planes Electrifly 45A* ESC, tested at $11.1\ V$ with the I_{max} and P_{max} set to $24\ A$ and $266\ W$, respectively. The motor has a K_v of $1400\ RPM/V$. It is designed to be operated in a $11.1\ V$ to $14.8\ V$ range and has an I_{max} and P_{max} of $25\ A$ and $370\ W$, respectively. Also, the ESC is designed to be used in a $7.4\ V$ to $14.8\ V$ range at a maximum of $45\ A$. We see that the three tests produce very similar results with all the quantities data repeating extremely well in the full range. The minor variation in the two data points in Test 3 showing a 4% variation in η_{mec} and $9\ W$ variation in P_{out_m} could very well be a bad data point where the motor was not loaded completely as shown by the corresponding drop of 0.15 *lb.-in* in Q_m.

Comparing the data for the two mec from Figures 25 and 27, we see that the second mec data repeats extremely well compared to the first one. Hence, we can

conclude that the variation in the performance in Figure 25 is just a characteristic of the mec combo and not an issue with the test system.

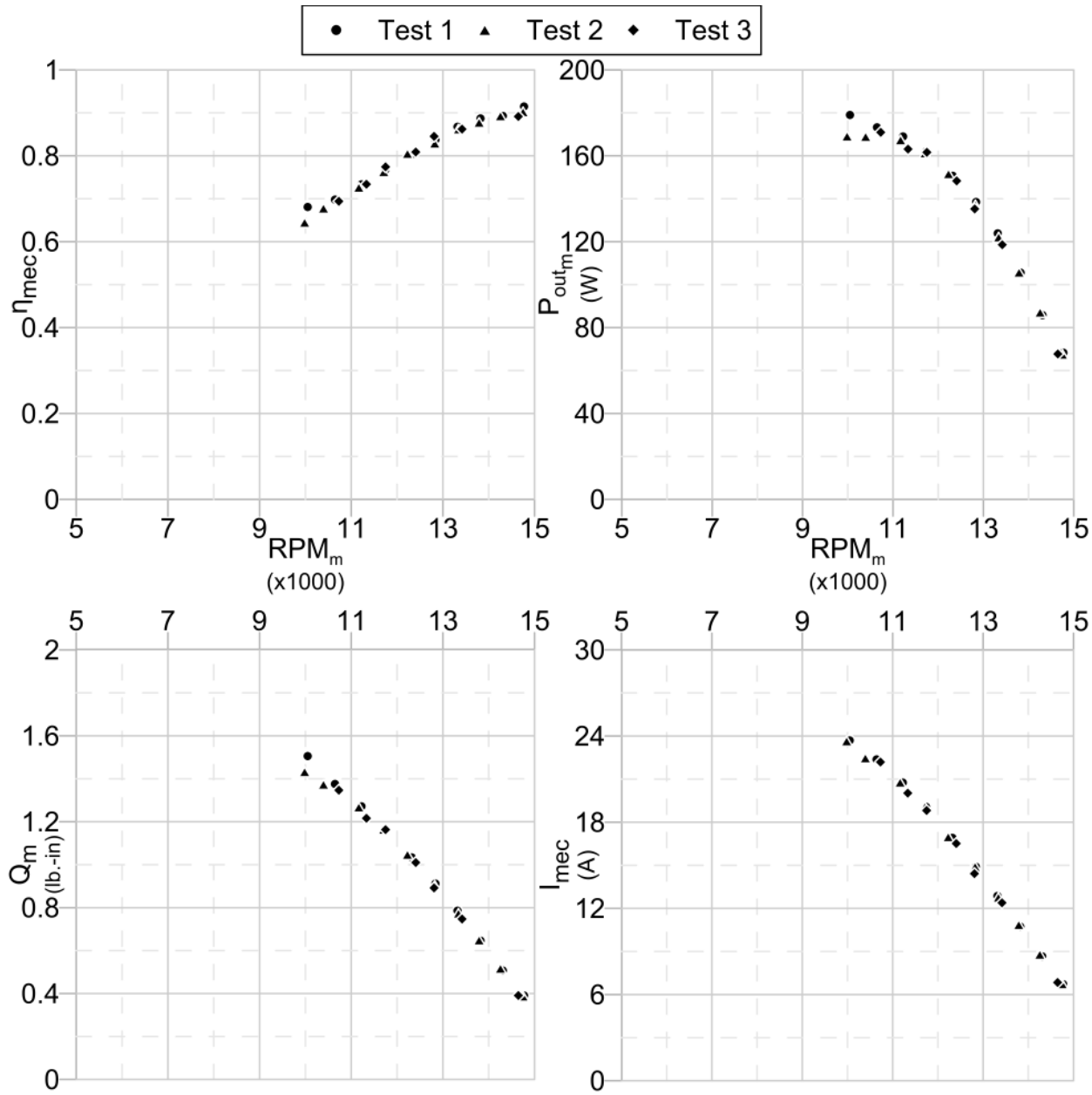

Figure 27. Performance data for the *Scorpion SII-2212-1400KV* with the *Electrifly 45A*, tested at $11.1\ V$.

Figure 28 shows the V_{mec} sensed by the voltage sensor during this test. Once again, the data repeats extremely well.

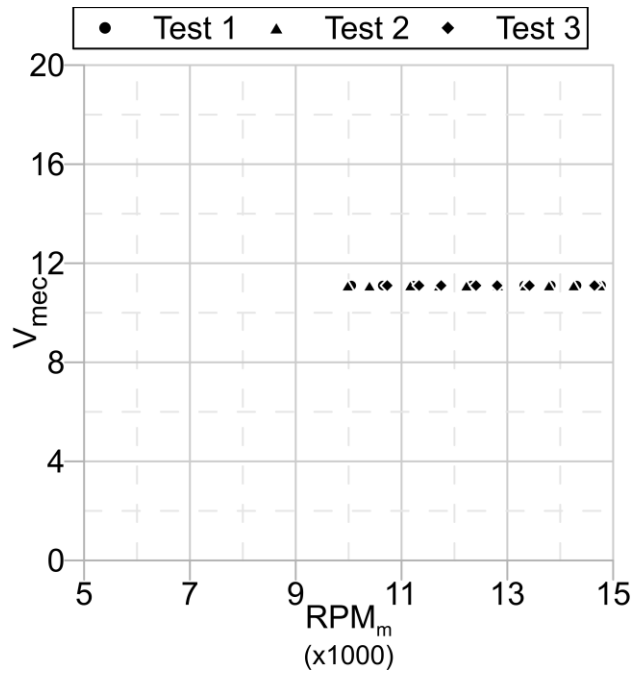

Figure 28. The sensed V_{mec} for the *Scorpion SII-2212-1400KV* with the *Electrifly 45A*, tested at $11.1\ V$.

Other than proving repeatability of the system, we can also see some general trend from this data. We see that both mec have high η_{mec} at high RPM_m, with it dropping as the P_{out_m} increases. The increase in P_{out_m} with drop in RPM_m, also corresponds to an increase in Q_m and I_{mec}, as expected.

Another test was also performed to validate the procedure. This involved starting the motor up at a high load and collecting data points as the load is decreased. The data obtained was found to be the same as those from the normal test, where the motor is started at zero load and the load increased. However, the latter which is the recommended procedure is significantly safer as the former could lead to the motor being loaded beyond its maximum limits on startup leading to motor stall. The latter also helps prevent the I_{max} and P_{max} being exceeded as the load can be carefully increased and the test stopped before the limits are hit.

5.2. Further tests

It is important to know the full scope of the test system. Hence, tests are conducted by varying test factors, to simulate meaningful variations to the mec and their operating conditions. These include, testing the same motor with a different ESC, testing the same mec at a different voltage (V_{mec}), and changing the throttle setting. A smaller and a bigger motor are also tested to obtain a wider array of data. All tests conducted uses safe variations. For example, using a motor with an ESC rated for a lower current, or running a motor or an ESC at a current greater than the specified I_{max} are not safe tests.

5.2.1. Varying ESC

The two motors from Section 5.1 are now tested with different ESCs. Also, since repeatability has already been proven, only two sets of tests are done for most of the setups.

Figure 29 shows the performance data for the *Great Planes Rimfire 400* brushless out-runner motor with the *Great Planes Rimfire 25A* ESC, tested at $11.0\,V$ with the I_{max} and P_{max} set to $13A$ and $143W$, respectively. The ESC is designed to be used in an $11.1\,V$ to $14.8\,V$ range at a maximum of $25\,A$. We see that the two tests produce very similar results, and these results are very similar to that from Figure 25. The repeatability here once again shows that the spread in the data in Figure 1 was caused by the specific mec.

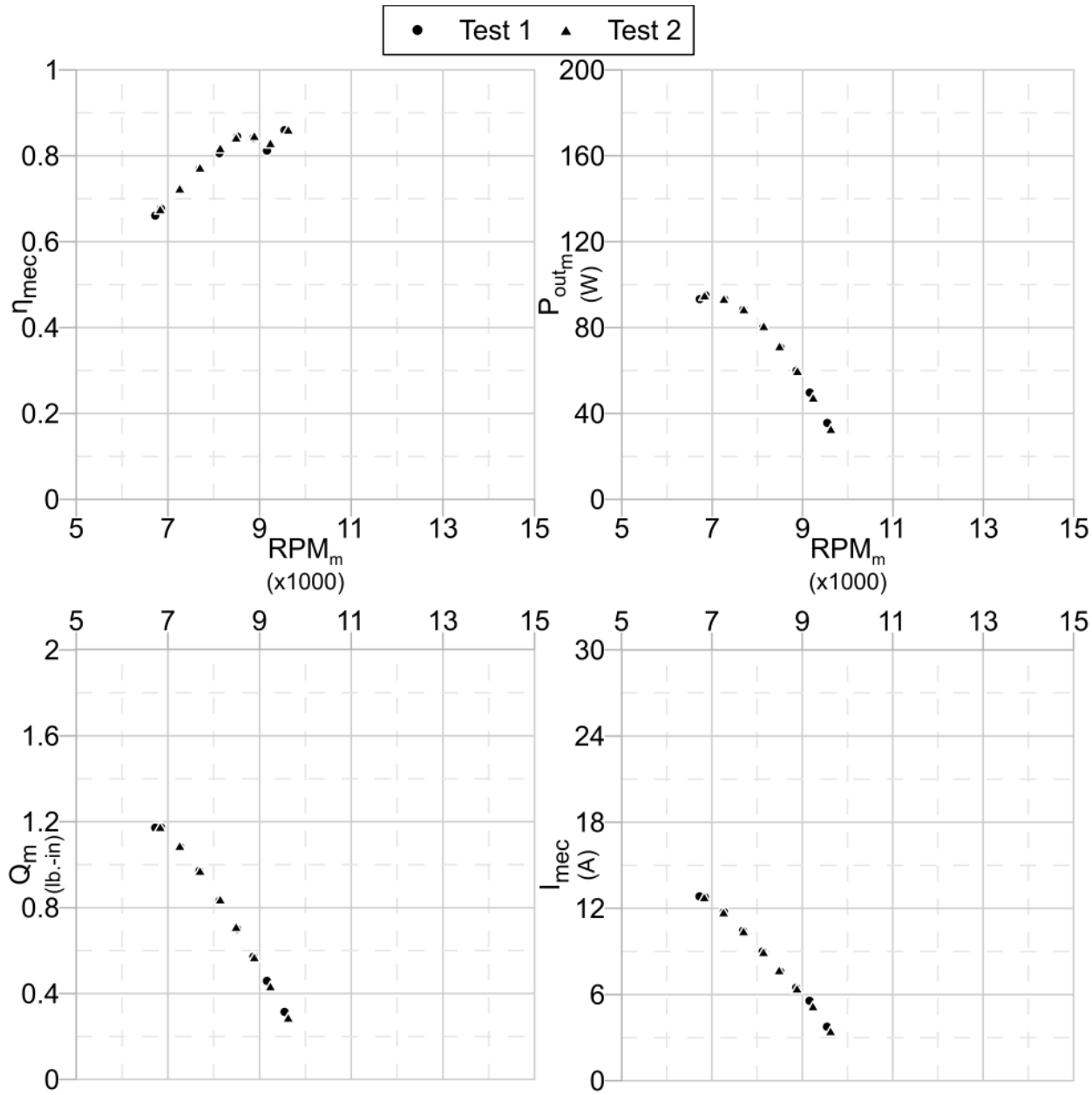

Figure 29. Performance data for the *Rimfire 400* with the *Electrifly 25A*, tested at $11.0\ V$.

Figure 30 shows the performance data for the *Scorpion SII-2212-1400KV* brushless out-runner motor with the *Castle Creations Phoenix Edge Lite 75A* ESC, tested at $11.1\ V$ with the I_{max} and P_{max} set to $24\ A$ and $266\ W$, respectively. The ESC is designed to be used in a $7.4\ V$ to $33.6\ V$ range at a maximum of $75\ A$. We see that the two tests produce very similar results, and these results are very similar to that from Figure 27.

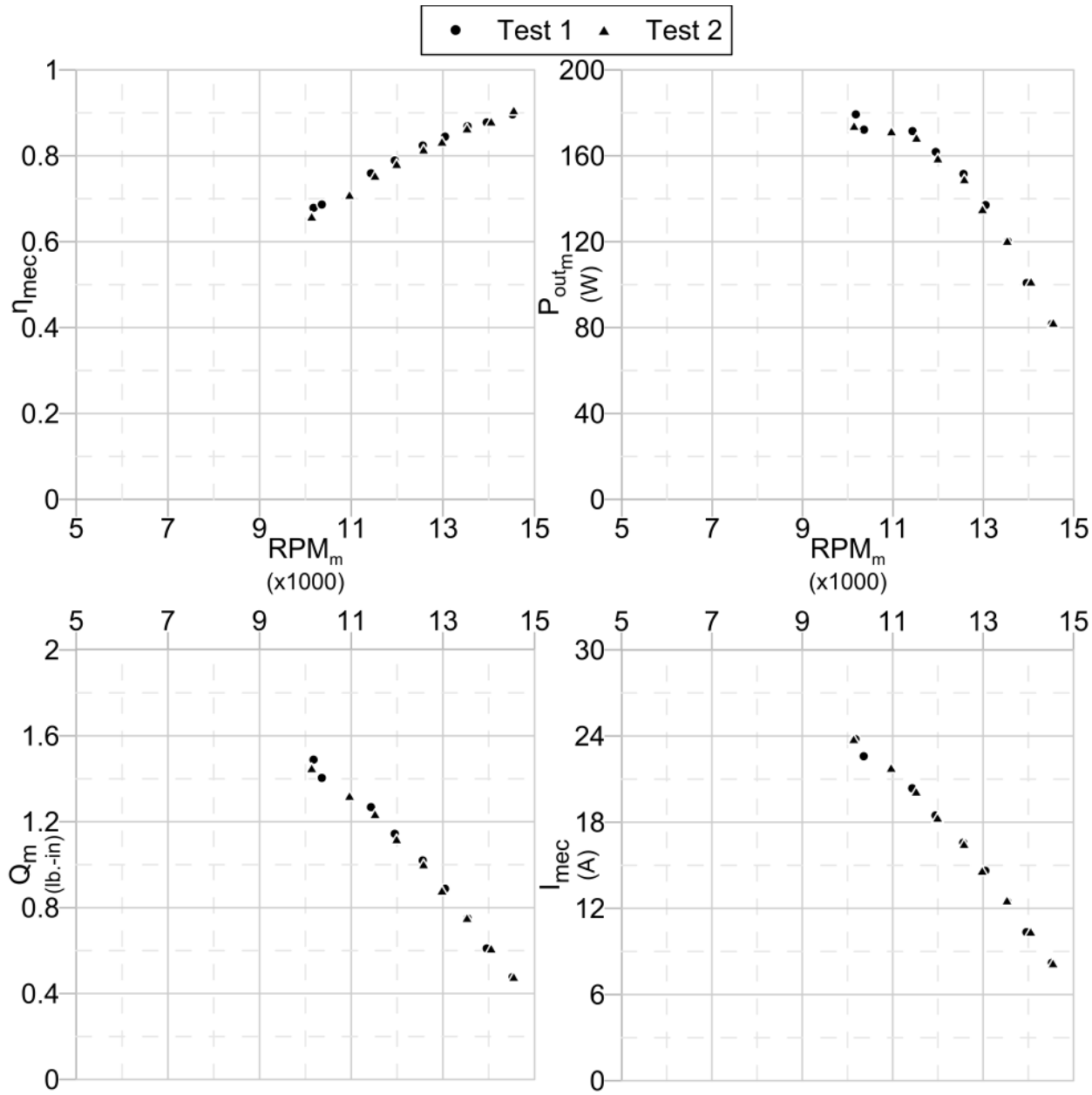

Figure 30. Performance data for the *Scorpion SII-2212-1400KV* with the *Phoenix 75A*, tested at $11.1\ V$.

Comparing Figures 25 and 29, and Figures 27 and 30, we see that changing the ESC has very minimal, if any, effect on the mec performance. Figures 25 and 29 might show that the *Electrifly 25A ESC* adds better stability to the performance to the system as

opposed to the *Talon 25A*. Figures 27 and 30 show that operating the *Phoenix 75A ESC* rated for much higher current at a lower current does not affect the efficiency.

5.2.2. Varying V_{mec}

The *Great Planes Rimfire 400* brushless out-runner motor with the *Castle Creations Talon 25A* ESC, is now tested at a lower V_{mec} of $7.4\ V$, with I_{max} and P_{max} set to $13\ A$ and $96.2\ W$, respectively. This data is presented in Figure 31. This setup performs till approximately $3{,}500\ RPM$. However, it was decided to cut off the plots at $5{,}000\ RPM$ for practicality as the former can be considered a very low RPM.

Comparing Figures 25 and 31, we see that the operating RPM is lower for the lower V_{mec}, as expected. Moreover, the Q_m and I_{mec} values remain very similar, although shifted on the RPM axis. These observations independently validate equations (10) and (12), respectively, showing that the RPM_m mainly depends on the K_v and the V_{mec} and the Q_m mainly depends on the K_t and the I_{mec}.

We can also see the variation between tests in the η_{mec} at the higher RPM_m in Figure 31, similar to that in Figure 25. This could once again be a result of this specific mec.

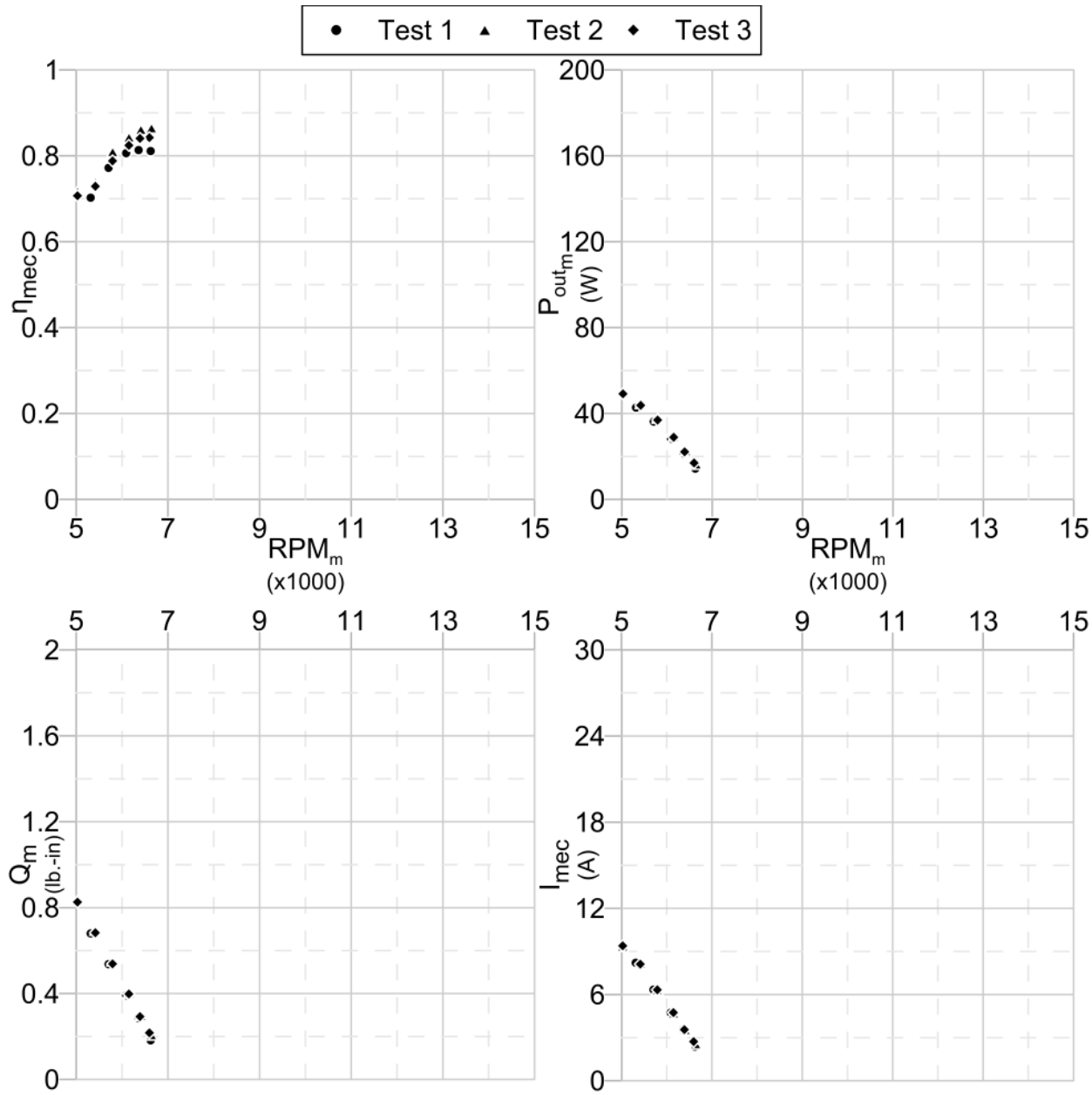

Figure 31. Performance data for the *Rimfire 400* with the *Talon 25A*, tested at $7.4\ V$.

5.2.3. Lower power motor

Figure 32 shows the performance data for the *Great Planes Rimfire 370* brushless out-runner motor with the *Castle Creations Talon 25A* ESC, tested at $11.1\ V$ with the I_{max} and P_{max} set to $12\ A$ and $133.2\ W$, respectively. The motor has a K_v of $1{,}000\ RPM/V$. It is

designed to be operated in a $7.4\,V$ to $11.1\,V$ range and has an I_{max} and P_{max} of $12.16\,A$ and $135\,W$, respectively. We see that the three tests produce very similar results, except for one data point in Test 2, at the highest RPM_m, which could be an outlier.

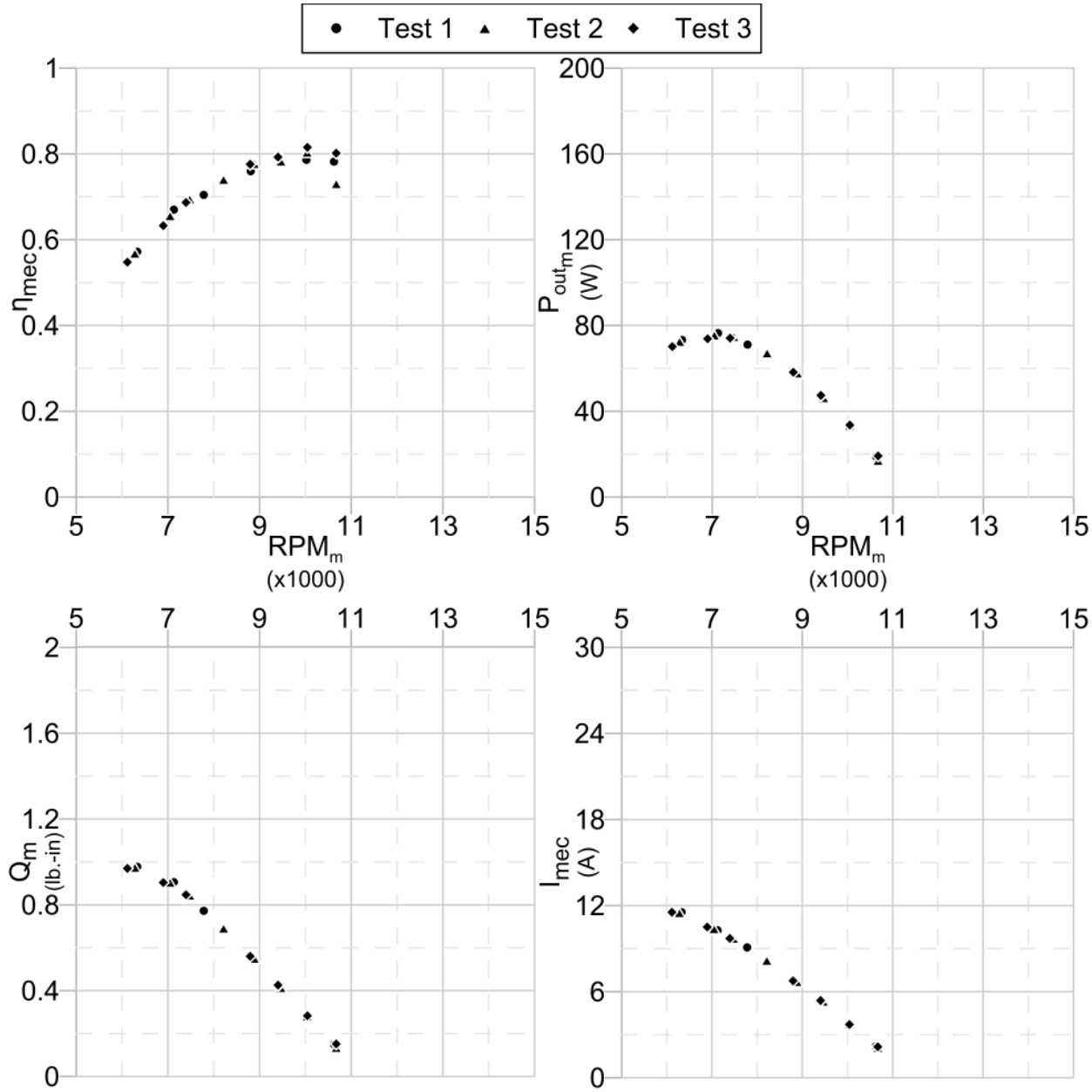

Figure 32. Performance data for the *Rimfire 370* with the *Talon 25A*, tested at $11.1\,V$.

5.2.4. Higher power motor

Figure 33 shows the performance data for the *Great Planes Rimfire .10* brushless out-runner motor with the *Great Planes Electrifly 45A* ESC, tested at $11.1\ V$ with the I_{max} and P_{max} set to $28\ A$ and $310.8\ W$, respectively. The motor has a K_v of $1{,}250\ RPM/V$. It is designed to be operated in a $7.4\ V$ to $11.1\ V$ range and has an I_{max} and P_{max} of $29.2\ A$ and $325\ W$, respectively. We see that the two tests produce very similar results. The spread in η_{mec} at RPM_m greater than $11{,}000\ RPM$, could once again be due to the characteristic of the specific mec.

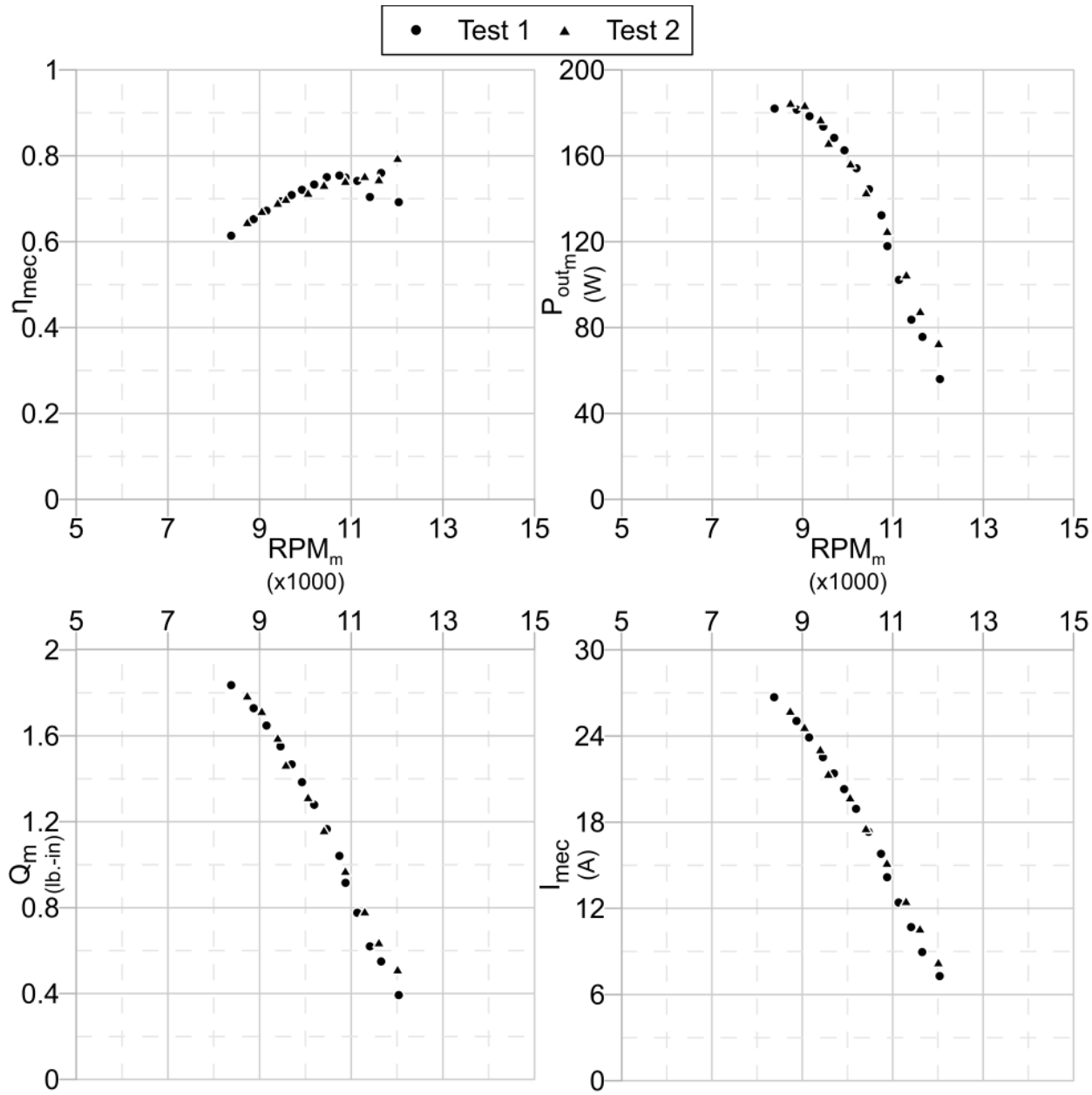

Figure 33. Performance data for the *Rimfire .10* with the *Electrifly 45A*, tested at $11.1\,V$.

5.2.5. Varying throttle setting

The *Great Planes Rimfire 400* brushless out-runner motor with the *Castle Creations Talon 25A* ESC, is tested at $11.0\,V$ with the I_{max} and P_{max} set to $13A$ and $143W$, respectively, at three different throttle levels – 100%, 75%, and 50%. Only one test is done

per throttle setting as we are mainly interested in the trend rather than the exact data. This data is shown in Figure 34.

We see that, as the throttle is decreased, the RPM_m decreases similar to when the V_{mec} is decreased. Moreover, the Q_m and I_{mec} curves remain the same, albeit being shifted on the RPM_m axis, similar to the decreased V_{mec} case of Section 5.2.2. Also, when the throttle is at 50%, most of the motor operation is below $5{,}000\ RPM$.

We also see that, the η_{mec} curve also drops with decreasing throttle setting. This is because of the drop in P_{out_m} caused by the drop in RPM_m, while V_{mec} and I_{mec} remains the same. Essentially, the ESC is limiting the voltage going into the motor by varying the frequency of the switching DC, as explained in Section 2.5.

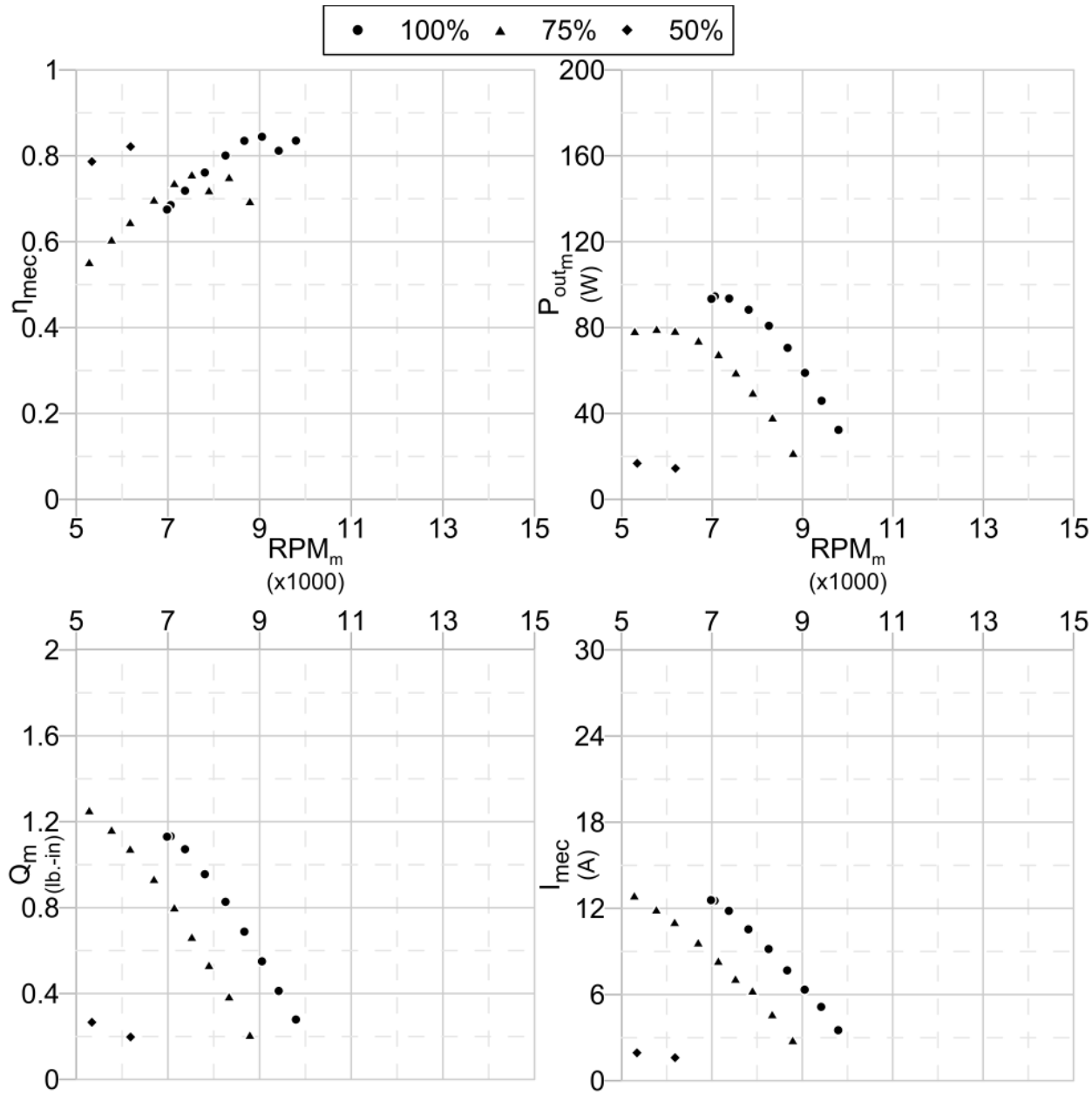

Figure 34. Performance data for the *Rimfire 400* with the *Talon 25A*, tested at $11.0\ V$ for varying throttle settings.

5.3. Quick comparison of motor-ESC combos

Finally, we can compile the data for the various motors on a single plot as shown in Figure 35. This provides a quick way to compare mec performance. Various ESC

combinations with the same motors have been left off, because of the minimal effect the ESC seems to have the performance in these tests.

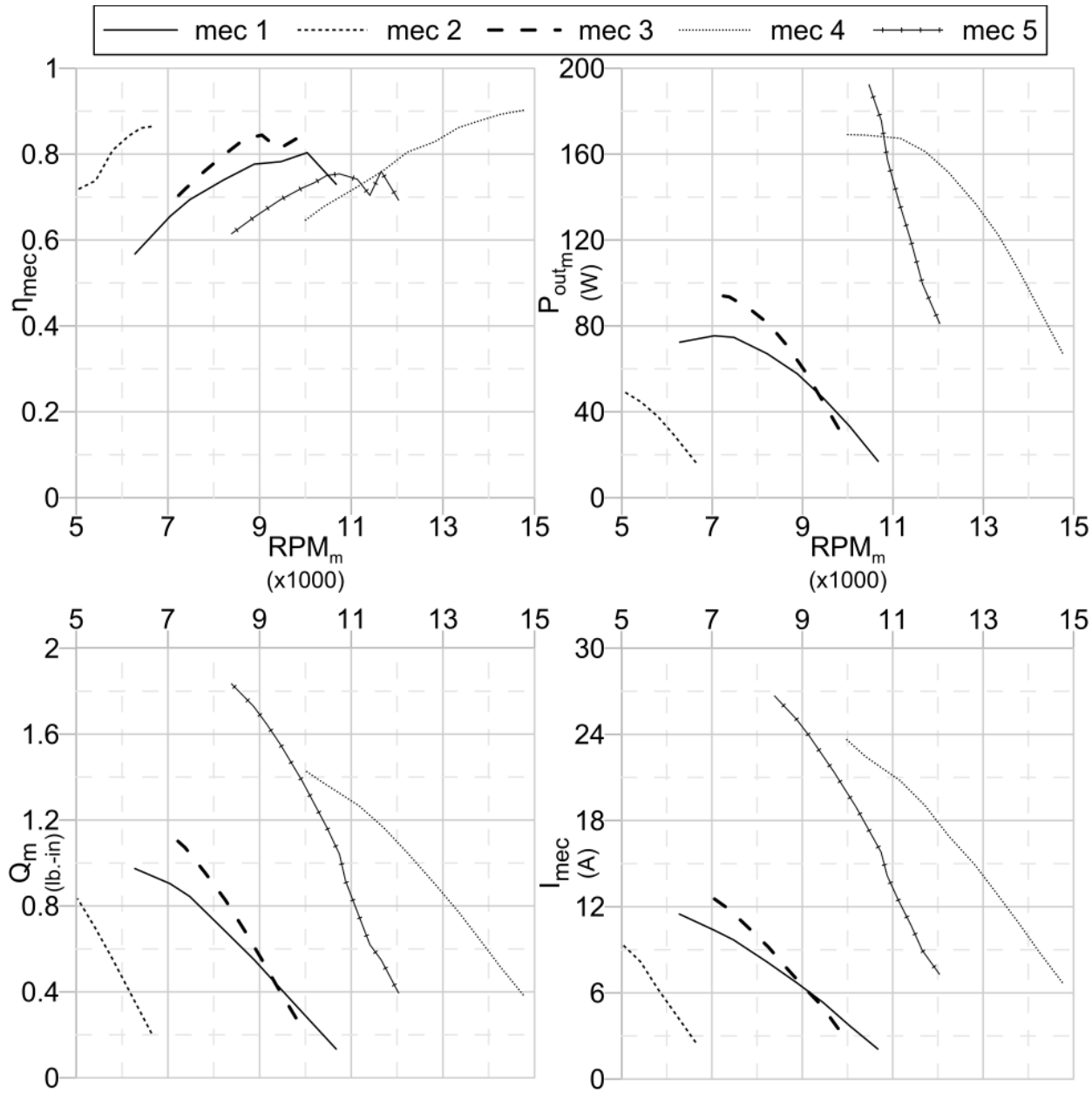

Figure 35. Comparison of performance data for all the tested motors. $mec1$ – Rimfire 370 + Talon 25A at $11.1V$; $mec2$- Rimfire 400 + Talon 25A at $7.4V$; $mec3$ - Rimfire 400 + Talon 25A at $11.0V$; $mec4$ – Scorpion SII-2212-1400KV + Electrifly 45A at $11.1V$; and $mec5$ - Rimfire .10 + Electrifly 45A at $11.1V$.

The combos shown on Figure 35 are as follows: $mec1$ – *Rimfire 370* + *Talon 25A* ESC at $11.1V$; $mec2$- *Rimfire 400* + *Talon 25A* ESC at $7.4V$; $mec3$ - *Rimfire 400* + *Talon 25A* ESC at $11.0V$; $mec4$ – *Scorpion SII-2212-1400KV* + *Electrifly 45A* ESC at $11.1V$; and $mec5$ - *Rimfire .10* + *Electrifly 45A* ESC at $11.1V$.

We see that $mec4$ has a higher efficiency across its range compared to that of the rest of the motors. However, it operates at higher RPM_m because of its higher K_v rating. Also, the P_{out_m} for $mec1$ and $mec4$ seem to plateau after which it remains approximately constant or drops. Hence, we see that a plot like this helps to quickly identify the characteristics of the mec. It can be used to determine if an mec is viable in a required RPM range or to check which mec would draw an I_{mec} below a specified value.

5.4. Other observations

This section discusses some secondary observations that were made during these tests.

5.4.1. Cold test case

It was found in multiple instances that if a motor is tested 'cold', i.e. if it has not been used for a while before it is tested, it produces a performance curve that is significantly different from every other test. The only way to replicate this would be to leave the motor and ESC unplugged for a few hours. These data were collected but have not been presented because, in a realistic case the motor is almost never run cold. Most UAV pilots check the throttle before flying to ensure that the motor and ESC is responding properly. This would take the motor through its paces and hence when the aircraft is flown, it will be performing at the actual performance level. Even if the motor is not

checked before the aircraft is flown, it should settle into its natural performance quickly and majority of the flight should once again happen in the actual performance level. Some examples of cold test cases are presented in Appendix B.

5.4.2. Temperature effects

All the tests were done at a T_r of $22°C$ to $23°C$. The T_m was monitored at the base of the stationary part of the motor and was found to hit up to $30°C$. However, no reliable signs of temperature dependence on motor performance were found. Some tests were also run with a compressed air line cooling the motor coil during the tests, and the data was found to be the same as the normal cases. However, this does not prove the absence of temperature dependence. It shows that any temperature dependence, if present, is hard to quantify.

5.4.3. Testing high power motors

The highest power motor presented here has a rating of $325\ W$. This is due to the characteristics of the load motor. The current setup uses a *Great Planes Rimfire .25* brushless out-runner motor as the load motor. This motor has a K_v of $1{,}000\ RPM/V$. It is designed to be operated in a $11.1\ V$ to $14.8\ V$ range and has an I_{max} and P_{max} of $43.9\ A$ and $650\ W$, respectively. Hence if the test motor is working at RPM greater than approximately $14{,}800\ RPM$, it would put the load motor outside its design range. Also, if the test motor has a power rating similar to the load motor, but a lower K_v, it would essentially have a Q_m higher than the load motor, which is once again not ideal. Hence to test motors at an RPM higher than approximately $15{,}000\ RPM$ or Q_m higher than the test

motor, we will need to use a load motor that is designed to work in the required range. It was found that a factor of 2.2 on the input power rating can alleviate the problem.

The test apparatus design allows to swap the load motor if required. Hence if a motor bigger than those tested here or a motor with higher RPM needs to be tested, the load motor can be swapped to a more suitable one.

5.4.4. Running a motor beyond its ratings

During these series of tests, some motors were run accidentally over its maximum rated current and power. As soon as the motor slightly exceeded the ratings, it would emit a white smoke and stop working. On further examination it was found that the motor windings were burnt and hence the motors were irreparably damaged. This shows that the I_{max} and P_{max} ratings are to be strictly adhered to, and it is safer to test slightly below these ratings.

CHAPTER 6

6. CONCLUSIONS

A test stand that facilitates the testing of DC electric motors under 750 W has been designed and a procedure for doing the same developed. From the results obtained, we can conclude that the test apparatus and procedure work as intended. We see that as long as a proper load motor is used, any motor-ESC combination can be tested to obtain good repeatable data. Moreover, the uncertainties in obtained data are reasonable, especially for engineering design purposes.

We see that this data can be used with the existing data for the other propulsion system components to characterize the full system. With the capability to obtain reliable data for the motor and ESC, a big gap in the prediction of propulsion system performance will be filled.

We can also conclude that motors need to be tested multiple times with the first 'cold' test disregarded, in order to ensure that the data is reliable.

The maximum current and power ratings for the motor also need to be strictly adhered to, and it is safer to test slightly below these ratings to prevent chance of damage to the test motor or even possibly the test apparatus.

Finally, we can conclude that the load motor should be selected carefully to ensure safe and reliable testing. A factor of 2.2 should be applied to the input power rating of the test motor when the load motor is selected.

CHAPTER 7

7. RECOMMENDATIONS

This section briefly discusses some recommendations that could be used to improve the system. These improvements were not performed because they were not deemed necessary. However, these could be used for future upgrades.

7.1. Torque sensor data rate

In Section 3.4.3, it is mentioned that the torque sensor is limited to a $10Hz$ data sampling rate because of the limitations on the HX711 amplifier. This can be improved using an analog load cell amplifier, which can then be connected to one of the ports on the 16-bit ADC. This would greatly increase the sample count and reduce the sampling time for this sensor. However, this upgrade would be expensive. Moreover, it was determined that even with the lower data rate, the read torque is reliable.

7.2. In-house current sensor

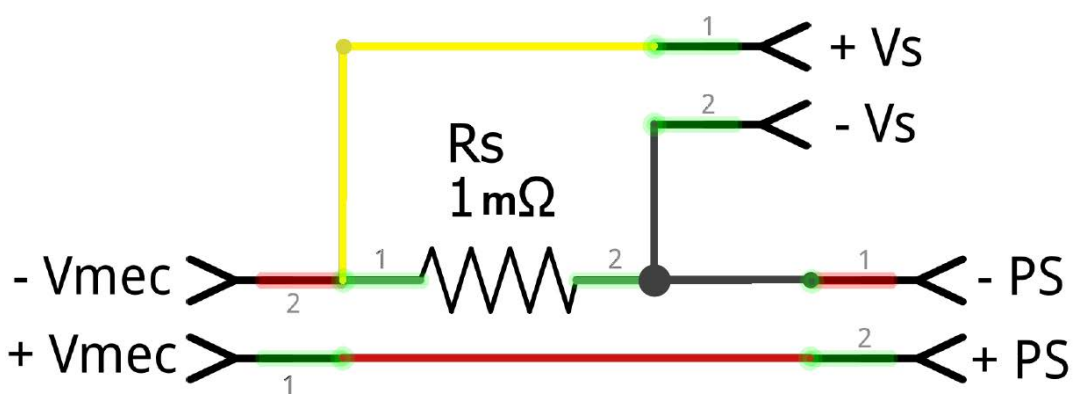

Figure 36. Schematic of a possible in-house current sensor.

From Section 3.6.2 and 3.7, we know that the current sensor is reliable and produces data with reasonable uncertainties. However, the manufacturer does not

produce this sensor anymore. If the current sensor needs to be replaced, it is recommended that a sensor be designed in house, as most off the shelf sensors cannot handle high currents. Figure 36 shows a circuit that was attempted. It works off of Ohm's Law and the output is described by equation (27), where V_{shunt} is the voltage across the shunt resistor, which is the same as the signal (V_s) from it, I_{shunt} the current flowing through it and R_{shunt} the shunt resistance, which is $1\ mOhm$. The shunt resistor used needs to be rated for high power (approximately $2.5W$), which can be backed off from equation (28). However, a $2W$ resistor can be used with a slightly lower maximum current of $44.7\ A$ or $40\ A$ to be safe.

$$V_{shunt} = I_{shunt} . R_{shunt} \tag{27}$$

$$P_{shunt} = I_{shunt}^2 . R_{shunt} \tag{28}$$

The sensor was calibrated and found to be linear, as expected. However, when connected to the ESC, its calibration would change and hence the readings would be meaningless. If a viable way is found to prevent this change in calibration, it would provide a good way to sense current.

7.3. Simplified torque sensor design

A simplified torque sensor could possibly be realized with some modifications to 'design d' from Section 3.4.3. Figure 37 shows the proposed design. Two load cells are sandwiched with good clearance between two plates. They are centered horizontally across the plates. The center of the load cells attached to the rear plate. The other end of the load cells is attached to the front plate at vertically opposite sides. The gray boxes show the location where the parts are attached.

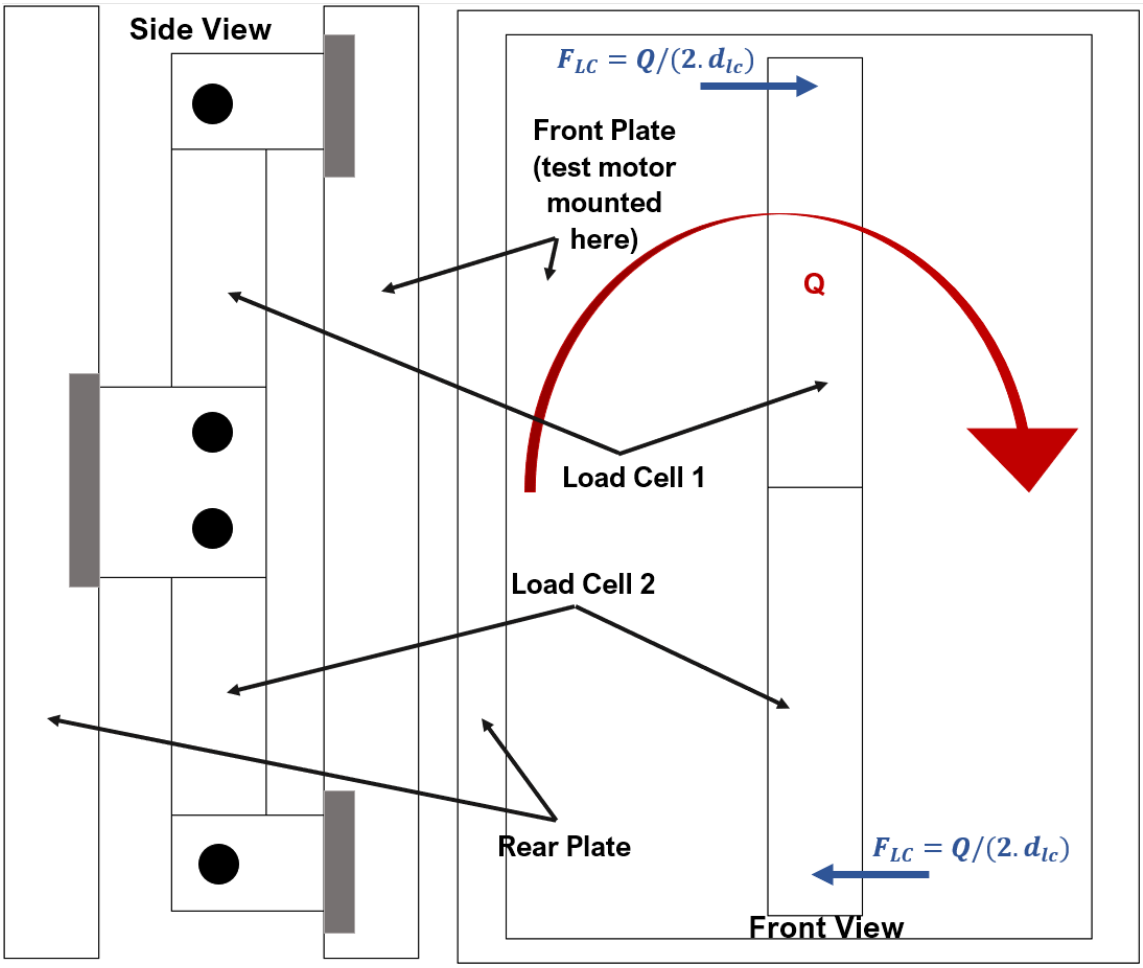

Figure 37. Schematic of a possible simplified torque sensor.

When a torque (Q) is applied to the front plate, a force of (F_{LC}) should appear in opposite directions on the two load cells of length (d_{lc}). These forces can be determined from both the load cells and together be used to find Q. If this design works as intended, it eliminates the moving components, i.e. the roller bearing, in the current design. It would also be quite a lot more rugged than the current design.

REFERENCES

REFERENCES

[1] Anderson, J. D., "Elements of Airplane Performance", *Introduction to flight*, McGraw-Hill Education, 3rd ed., New York, NY, 1989, pp. 259-353

[2] Merchant, M. P., *Propeller Performance Measurement for Low Reynolds Number Unmanned Aerial Vehicle Applications*, Wichita State University, 2005.

[3] Brown, M. Brushless RC Motors [Online], http://www.hooked-on-rc-airplanes.com/brushless-rc-motors.html, retrieved Oct. 2018.

[4] Boucher, R. J., *The Electric Motor Handbook*, 2nd ed., AstroFlight, Inc., 1995.

[5] "An Electronic Speed Control Primer", *Sailplane & Electric Modeler Magazine*, Sept. 30, 1997, http://www.stefanv.com/electronics/escprimer.html, retrieved Oct. 2018.

[6] Agarwal, T., *Introduction to Electronic Speed Control (ESC) Working and Applications* [Online], https://www.elprocus.com/electronic-speed-control-esc-working-applications/, retrieved Oct. 2018.

[7] Kuphaldt, T. R., "Divider Circuits and Kirchhoff's Law," *Lessons In Electric Circuits: Voume I -DC* [Online] http://www.ibiblio.org/kuphaldt/electricCircuits/DC/DC_6.html#xtocid33340, 2006, retrieved Oct. 2018.

[8] *Angular contact ball bearings, double row* [Online], http://www.skf.com/group/products/bearings-units-housings/ball-bearings/angular-contact-ball-bearings/double-row-angular-contact-ball-bearings/double-row/index.html?designation=3205%20A, retrieved Oct. 2018.

[9] Wheeler, A. J., and Ganji, A. R., "Experimental Uncertainty Analysis," *Introduction to engineering experimentation*, 3rd ed., Prentice Hall, Boston, 2009, pp. 199-202.

APPENDICES

APPENDIX A

WSU MOTOR TESTING SYSTEM USER MANUAL

OVERVIEW

We test an electric motor by physically connecting it to another motor called the load motor. The load motor is controlled by a resistive system called an electronic load. The electronic load is used to slowly increase the load applied to the test motor. As a result, the test motor draws more current.

Hence to test these motors, prepare a test matrix with a range of currents from low to high (~1 A below your motor's rated limit), so you get a full performance curve. Approximately ten (10) data-points should be enough.

It is recommended that you test a motor at least thrice at ~15-20 min intervals. The first 'break-in' test may result in data that is slightly different from the rest of the tests, which is normal. The actual motor performance will be that obtained after the break-in.

PRE-TEST PREPARATIONS

Motor limits

In order to safely test the motor, the voltage, max. current and max. power ratings for the motor and ESC needs to be known. Find these from the manufacturer and not a vendor.

It is recommended that the tests be performed at the nominal voltage of the battery, or the voltage determined from the battery test, and not the fully charged voltage.

If the maximum current is not provided, it can be calculated using equation (1), where V_{max} is the highest nominal voltage for which the motor is rated. e.g.: If the motor can use up to a 3S LiPo battery, use 11.1 V and not 12.6V.

$$I_{max} = \frac{P_{max}}{V_{max}} \tag{1}$$

If the motor is to be tested at a voltage lower than V_{max}, recalculate P_{max} using the obtained or provide I_{max} with equation (2).

$$P_{max} = V_{lower} . I_{max} \tag{2}$$

It is highly recommended that you not take the motor to its maximum current and power limits. It is safer to choose a maximum current ~0.5-1 A below the maximum continuous rating and calculate the power for that.

Write down the test voltage (V_{test}), I_{max} and P_{max}, and have them ready for your test.

Mounting the motor

The pattern needed for the test motor mount is as shown. You can use this to manufacture the required mount. It is recommended that the mount be laser cut from 1/8” light ply.

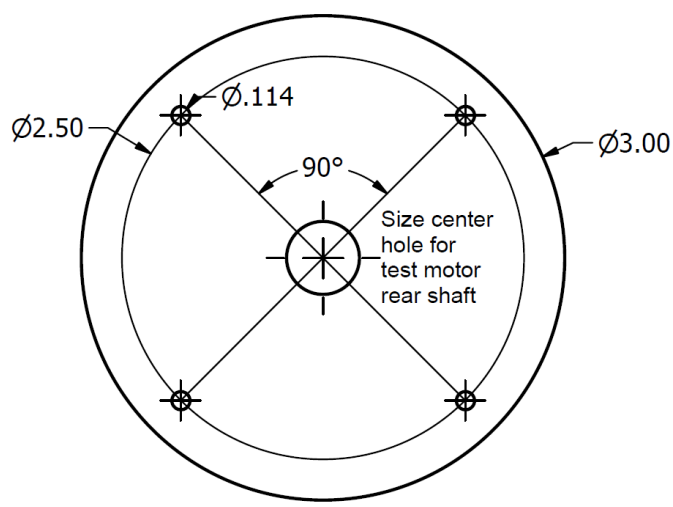

Test motor mount pattern. All dimensions are in inches.

Flash drive

The only way to get data from the test stand is using a flash drive. It **only supports USB**

2.0 flash-drives. It is recommended that you create a folder specifically for your motor tests, so the data can be easily accessed.

<u>The data acquisition WILL NOT be able to read USB 3.0 devices</u>.

DO NOT plug any device that require extra power like external HDDs, SSDs, etc., into the data acquisition system. This will lead to the sensors being switched OFF.

Linking the motor

We use ¼ drive sockets to link the test motor to the load motor. In order to do this, you will need to fit the motor with a prop shaft that has **a right-handed nut**. Use spacers to move the nut to the tip of the shaft. If you are using friction fitting prop shafts, put in spacers and ensure that the shaft doesn't spin independently from the motor. A few examples of prepared shafts, and a link with 2 sockets and the steel bar-link are shown.

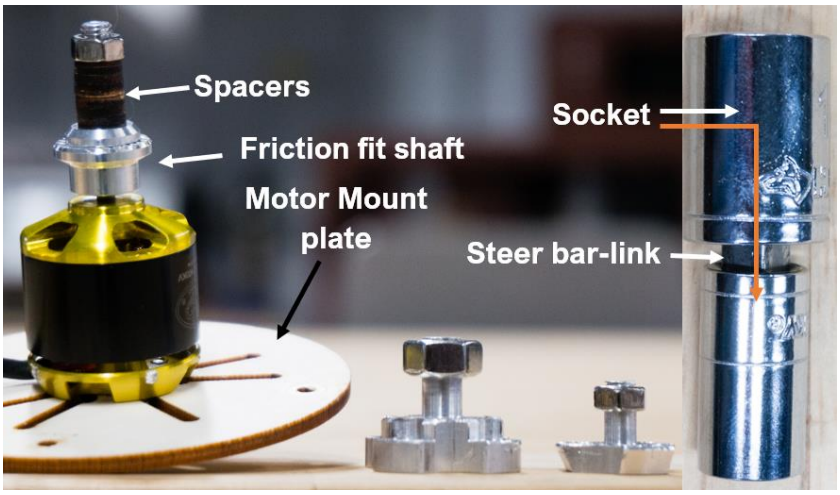

Prepared motor shafts (right) and a link with two sockets and the steel link (right).

Test Procedure

The locking pin should be in at all times, until specifically instructed to take it out.

i) Before you start, open the test section door and ensure that the load motor is on tight. If not, have someone fix it for you. When done close the door.

ii) Switch the test stand ON using the switch on the right of the stand and wait for the system to completely boot up. This could take around 2-3 minutes.

iii) Plug in your flash-drive to the USB port and check if the ‘Removable medium is inserted’ window pops-up.

If the system cannot read your flash-drive, make sure you use a flash-drive that it can read.

Hit cancel on the ‘Removable medium is inserted’ popup and return to the desktop.

iv) Switch the power supply and load on using the rockers on their left side.

DO NOT press the On/ Off buttons on the devices until asked to.

v) Click the ‘Meter’ button on the power supply to view the V and I settings. The green backlight on the button should turn OFF in this mode.

vi) Click V-set and use the num-pad to set V_{test}. Hit Enter when done.

vii) Click I-set and type in I_{max}. Hit Enter when done.

viii) Click Shift> I-set and type in P_{max}. Hit Enter when done.

ix) Ensure that the V and I settings are right.

x) Click the 'Meter' button.

This will take you to the Metering mode. The green LED on the 'Meter' button should turn ON, and the screen should read 0V and 0A.

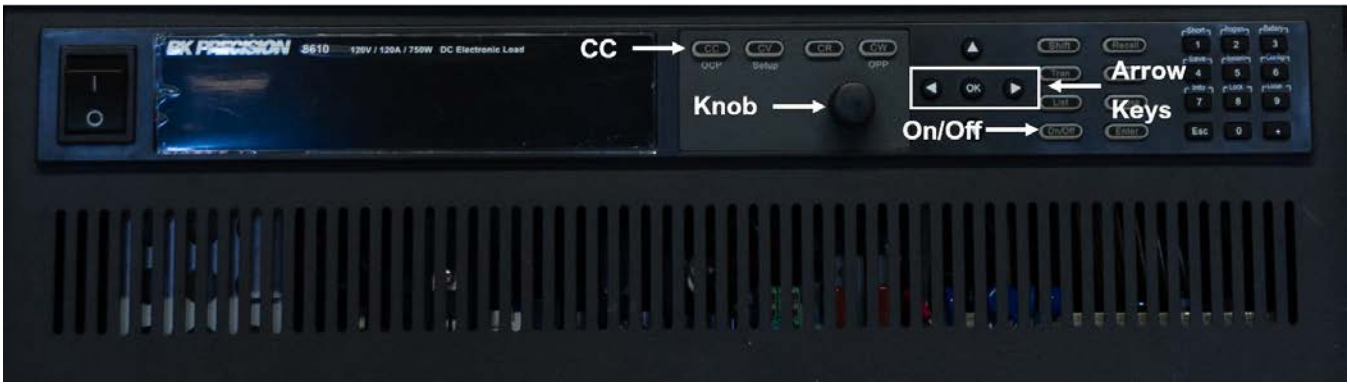

xi) Now look at the Electronic Load (load) and ensure that it is in CC (Constant Current) mode.

The CC button should be green. If not, click the button to turn it into CC mode.

The screen should reflect the same and should once again read 0V and very close to 0A. If not hit 0>Enter.

xii) Start the Motor Test App on the desktop.

You need to double click the icon and it could take a bit of effort for it to register the double-click properly.

xiii) Agree to the requirements.

xiv) Ensure that the locking pin is in.

xv) Mount the motor to the motor mount with the motor wires facing out, and lightly torque the nuts by hand.

xvi) Plug in your ESC to the power cable.

Use the provided ESC box if necessary.

xvii) Plug in the ESC signal cable.

Ensure that the Ground (-) and Signal (S) wires match up – White/ Yellow to White, Black/ Brown to Black.

xviii) Plug the ESC to the motor.

xix) Hit Next.

xx) Turn the power output ON using the On/ Off button on the power supply.

The screen on the supply should now read the V_{test} and close to 0A. In reality it could be ~0.2-0.5 A.

xxi) Wait for the ESC to initialize.

This is usually indicated by a series of beeps. Refer to the manufacturer for more info on this.

xxii) If your ESC needs to be initialized manually, use the on-screen throttle slider to do so.

Different ESC's have different requirements. Refer to the manufacturer for more info on this.

xxiii) Hit Test Motor to ensure that the motor is spinning counter-clockwise. If not, switch <u>any two wires</u> from the ESC to the motor and test again.

xxiv) Hit Next. The system now quickly sweeps the throttle from 0 to 100 %, and back to 0, to ensure that the ESC response is right. If you feel like the response is not characteristic of such a sweep, ensure that all your wirings and settings are right.

xxv) Now select the folder on your flash drive where you want the output saved. Ensure you double click into the folder.

The system opens to the folder where the flash-drive is. It should be the only folder in the default file-path.

The displayed name need not be the same as your flash-drive's actual name.

xxvi) Write down the output file name.

xxvii) Hit Next.

xxviii) Slide the load side tower towards the test motor and link them using appropriate sockets and a provided ¼" steel stock.

DO NOT put axial pressure on the test motor.

xxix) Use a small strip of masking tape to hold the two sockets in place w.r.t each other.

xxx) Tighten the load side tower using a 5/16" Allen drive.

xxxi) Take out the locking pin and LIGHTLY tap the moment arm to ensure that it is touching the load cell.

xxxii) Ensure that all the wires are out of the way, and close the test section door.

xxxiii) Hit 'TARE' to tare the load cell.

xxxiv) Once tared, hit the Next button. This will take you to the Data Collection page.

xxxv) If testing at a throttle other that max throttle (100 %), tick the radio box on the right side and use the slider to set the required throttle setting.

xxxvi) Hit ‘TURN MOTOR ON’.

It takes ~2 s to turn the motor completely on. Once fully started, the button should turn RED and the status light (the box right under the said button) under it should turn green.

xxxvii) Turn the load on using the ON/ OFF button on the electronic load.

xxxviii) SLOWLY increase the load using the knob, while watching the input current and power on the power supply.

You can increase the load by 1/10th increments by moving the cursor using the arrow keys. Be extremely careful while increasing the load and DO NOT increase it past the motors’ limits.

xxxix) Use the ‘Acquire Data’ button to get the data points at the necessary input currents. Once a data point has been acquired, the reading on the screen should update to reflect the same.

xl) Keep increasing the load and obtaining data points till the input power is close to the max limits. DO NOT attempt to get it to reach the limits. Instead, take your final point ~0.5 – 1 A below the limits.

xli) Once enough data points have been taken, hit ‘TURN MOTOR OFF’.

It takes ~2 s to turn the motor completely off. Once fully off, the button should turn GREEN and the status light under it should turn RED.

xlii) Turn OFF the power supply and load using the On/ Off buttons.

xliii) Open the test section door.

xliv) Put the locking pin back in.

xlv) Hit Next to finish the test.

xlvi) If taking more data, hit ‘Collect more Data’. Otherwise, hit Quit to finish tests.

xlvii) If taking more data, let the motor cool down for ~15-20 mins.

xlviii) When done, eject your flash-drive using the button on the top-right corner on the desktop.

xlix) When completely done, shut down the data acquisition system using the raspberry pi logo on the top left corner.

l) Turn off the power supply and load.

If the fans on the load or the power supply are running, wait for them to turn off before turning the system off.

li) Finally, turn the test stand OFF.

APPENDIX B

COLD TEST DATA

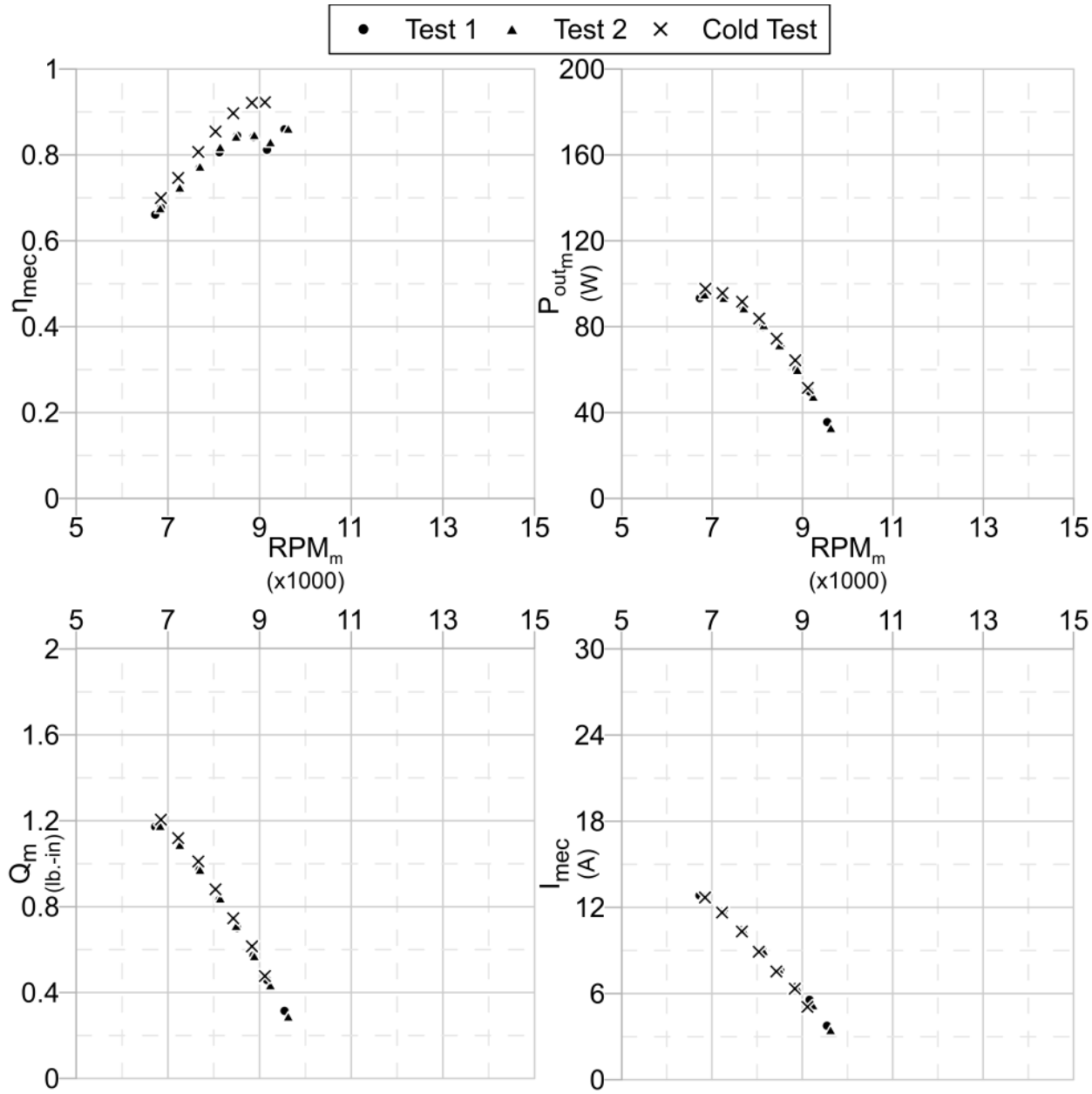

Figure 38. Performance data for the *Rimfire 400* with the *Electrifly 25A*, tested at $11.0\ V$ along with the cold test data. We can see that the cold test performance varies significantly from the other tests.

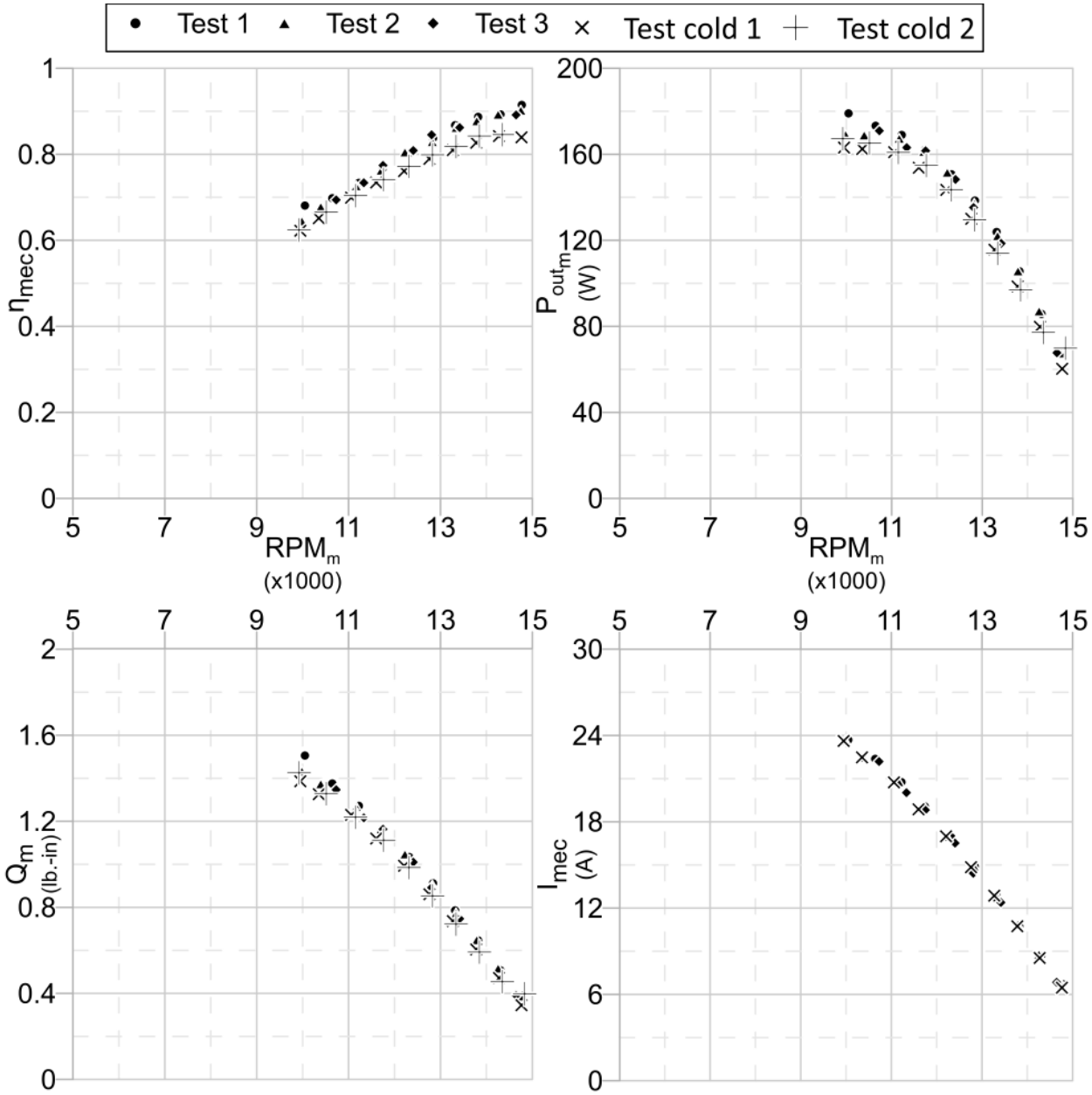

Figure 39. Performance data for the *Scorpion SII-2212-1400KV* with the *Electrifly 45A*, tested at $11.1\ V$ along with the cold test data. Once again, the cold test performance varies significantly from the other tests.